Check for updates

State of the art methods and challenges of luminescent metal–organic frameworks for antibiotic detection

Rongrong Yuan[a] and Hongming He 🆔 *[b]

Metal–organic frameworks (MOFs) are a burgeoning class of crystalline materials constructed from metal cations/clusters and organic ligands with various potential applications. Thus, luminescent MOFs display potential applications in smart sensing with excellent sensitivity, accuracy, anti-jamming, stability, and selectivity. MOFs possess their intrinsic luminescent property from metal cations, organic ligands, and other luminescent species *via* ingenious design and post-modification. Luminescent MOFs can be used as advanced detection materials for various antibiotics through their luminescent signal response, including the emission intensity and location. Herein, for the first time, we intend to provide a comprehensive overview on the state-of-the-art methods and challenges of antibiotic detection by luminescent MOFs.

1. Introduction

There are nearly 260 antibiotics, belonging to 20 classes, that have been synthesized and used in our life.[1] They have multifarious chemical compositions and structures, including intermediate metabolites and degradation products from parent compounds.[2] The global annual usage of antibiotics extends over 100 000 tons, which are extensively used in both human and veterinary drugs for the treatment of microbial and bacterial infections.[3,4] Only a tiny number of the therapeutic human and veterinary antibiotics can be absorbed and metabolized by the body. Thus, a massive amount of consumed antibiotics (50–90%) are excreted through urine and feces.[5,6] Subsequently, antibiotics and their metabolites enter the water environment through various ways. The common water purification process is almost invalid for removing antibiotics and their metabolites. The residual antibiotics enable the continuous selection of antibiotic-resistant bacteria with antibiotic-

[a]Department of Materials Science and Engineering, Jilin Jianzhu University, Changchun 130118, P. R. China
[b]Tianjin Key Laboratory of Structure and Performance for Functional Molecules, College of Chemistry, Tianjin Normal University, Tianjin 300387, P. R. China. E-mail: hehongminghz@163.com, hxxyhhm@tjnu.edu.cn

Rongrong Yuan obtained her Bachelor degree in Chemistry from Tsingdao University of Science and Technology in 2011. She then joined Professor Guangshan Zhu's research group for her Master and Ph.D. programs, mainly working on the targeted synthesis of porous organic frameworks for gas storage and separation. After receiving her Ph.D. degree in 2016, she became a lecturer at the Department of Materials

Rongrong Yuan

Science and Engineering, Jilin Jianzhu University. Her research interests focus on the synthesis, structure, and functions of porous materials.

Hongming He received his Bachelor degree in Materials Chemistry from Heilongjiang University, China in 2011. In the fall of 2011, he joined the research group of Prof. Guangshan Zhu for his Ph.D. program at Jilin University, China and received his Ph.D. degree in 2016. He is currently an assistant research fellow in the College of Chemistry in Tianjin Normal University. His current research focuses on the

Hongming He

development of porous functional materials for energy and environmental-related applications.

This journal is © the Partner Organisations 2020

Inorg. Chem. Front., 2020, **7**, 4293–4319 | **4293**

resistant genes.[7,8] In general, bacteria have two kinds of resistance towards antibiotics, including intrinsic and acquired resistance. The intrinsic resistance occurs naturally in organisms. Nevertheless, the acquired resistance is an evolution from sensitive to resistant bacteria by virtue of the gene mutation in DNA. Actually, the underlying mechanism of the increasing drug resistance remains uncertain. The uncontrolled misuse of antibiotics all over the world causes antibiotics to become ineffective to patients with viral infections, leading to more efforts in the development and synthesis of novel and efficient antibiotics with huge expenditure. There were more than 2.8 million cases and approximately 35 000 deaths in USA in 2019, which triggered the multidrug-resistant bacteria and fungus.[9] In this context, some countries, especially advanced nations, have developed and perfected the relative antimicrobial stewardship regulations to optimize the antibiotic use and reduce the inefficient consumption. Antibiotics raise a host of thorny environmental and health issues, because they can preserve their biological activation for a long time to affect non-target living tissues and organs. It is unfortunate that various antibiotics are found in agricultural, sideline products, rivers, drinking water, and underground water, which can infiltrate bionts by going up the food chain.[10] In light of the abovementioned issues, it is of essence to seek a highly efficient approach for accurate detection of antibiotics.

Multifarious techniques and materials have been developed to detect target antibiotics in recent years, such as gas chromatograph-mass spectrometry,[11] liquid chromatography–mass spectrometry,[12] luminescence,[13] electrochemistry,[14] and micellar electrokinetic capillary chromatography.[15] Thus, luminescence detection has attracted a great deal of attention due to the operator simplicity, low cost, quick response, preferable reproducibility, and sensitivity.[16–18] To date, various types of luminescence materials have been implemented in the detection of antibiotics.[19–23] In recent times, metal–organic frameworks (MOFs) have been a vigorous manifestation of crystalline-extended materials constructed by the coordination assembly of metal cations/clusters and organic ligands. MOFs have a wealth of advantages with high surface area, molecular- or atomic-level modulability, preferable designability, and structural diversity, resulting in their potential applications in gas sorption,[24,25] chemical sensors,[26,27] heterogeneous catalysts,[28,29] and biomolecular immobilization.[30,31] Luminescent MOFs (LMOFs) are a major category of MOFs, which are considered to be potential candidates as sensor materials to detect multiple substances, including heavy metals,[32] explosives,[33] and toxicants.[34] Compared with other luminescence materials, LMOFs have numerous excellent advantages, including multiple light sources, large Stokes shift, high luminance, stability, and host–guest interaction. The porous nature of LMOFs can enrich the guest analyte in LMOFs by capturing the trace analyte to enhance the sensing performance. Thanks to the special photophysical characteristics of MOFs, the signal transduction in the luminescence detection approach is mainly attributed to the photo-induced electron transition (PET) from n to π and from π to π*, accorded with the constitutes and structures of LMOFs.[35] Most LMOFs are prepared by using conjugated aromatic organic building ligands decorated with functional sites, so the multitudinous n and p electrons in LMOFs favor the signal transduction performance.[36] Furthermore, the inorganic cations/clusters in LMOFs remarkably play a positive role in the luminescence property, mainly involving rare earth- and other transition metal–inorganic nodes.[37] Hence, the luminescence property of LMOFs can be well designed and investigated because of the hybrid nature. Also, the inherent pores of MOFs are considered as host materials to trap functional advanced substances (e.g., Ln^{3+},[38] carbon dots,[39] and rhodamine B[40]) through host–guest chemistry to fabricate hybrid composites with a variety of luminous sources. On the other hand, porous LMOFs have the freely accessible space to facilitate the enrichment of analytes in pores, which can increase the detection effect by reason of the photophysical interaction between host MOFs and guest analytes. The rational design and construction of these compositions in LMOFs can make the most of their advantages to achieve superior detection performance. Although a large number of reviews have summarized the luminescence sensing applications of LMOFs,[41–43] there is still no review in regards to the antibiotic detection by LMOFs. Therefore, we focus on providing an overview of LMOFs as luminescence sensors toward various antibiotics. Since 2016, the first case was reported by Zr(IV)-based LMOFs to realize the highly efficient detection of antibiotics in water by luminescence quenching.[44] To date, more and more LMOFs based on multiple luminescent sources have been designed and synthesized to detect antibiotics (Table 1). In this review, some representative works have been highlighted and discussed in detail, which are divided into five categories, as follows: (1) LMOFs based on luminescent organic ligands; (2) LMOFs based on luminescent metal nodes; (3) Ln(III)-doped or adsorbed/linked lumophore-based LMOFs; (4) metal–organic gel-based luminescence sensor, and (5) LMOF thin film-based luminescence sensor. Eventually, we hope to provide a latest roadmap in the luminescence detection of antibiotics by LMOFs for the readers after reading this review.

2. LMOFs based on luminescent organic ligands

Luminescence organic ligands play a significantly important role in the construction of LMOFs, and have a noticeable effect on the detection of targeted analytes. In particular, bridging organic ligands with a rich π-electron aromatic nucleus are the uppermost candidates to contribute the luminescence property of LMOFs, including tetraphenyl ethylene-,[45] pyrene-,[46] and biphenyl-based ligands.[47] In comparison with other ligands, such conjugated organic ligands have the excellent property in the absorption of light as excitation energy to induce the radiative transition. In addition, n → π* and π → π* electron transitions are thought to be the main cause of the luminescence

4294 | Inorg. Chem. Front., 2020, 7, 4293–4319

This journal is © the Partner Organisations 2020

Table 1 Detection of antibiotics by LMOFs

MOF	Luminescence source	Analyte	Media	K_{sv} (M^{-1})	LOD	Ref.
BUT-12	Ligand	NFZ	Water	3.1×10^5	58 ppb	44
BUT-13	Ligand	NFZ	Water	7.5×10^4	90 ppb	
V-102	Ligand	NFZ	Water	6.38×10^4	0.2 ppm	49
$[(Zn_4O)_2(PDDA)_6(H_2O)_2]\cdot10DMF$	Ligand	NFT	DMF	1.16×10^5	—	51
	Ligand	NFZ	DMF	6.08×10^4	—	
$[Cd_4K_4(TADA)_4(H_2O)_{12}]\cdot6DMF$	Ligand	MDZ	DMF	1.16×10^5	—	52
$[NH_2(CH_3)_2]_4[Zn_3(HBDPO)_2(SO_4)_2]$	Ligand	NFZ	DMF	4.5×10^4	—	53
	Ligand	NFT	DMF	4.9×10^4	—	
$[Cd_3(TDCPB\cdot2DMAc\cdot DMAc\cdot4H_2O]$	Ligand	NFT	DMF	1.05×10^5	—	54
	Ligand	NFZ	DMF	7.46×10^4	—	
$[NaCd_2(L)(BDC)_{2.5}]\cdot9H_2O$	Ligand	NFZ	DMF	5.06×10^4	162 ppb	55
	Ligand	NFT	DMF	3.57×10^4	274 ppb	
	Ligand	FZD	DMF	1.83×10^4	494 ppb	
$[Cd_2(L)(2,6\text{-}NDC)_2]\cdot DMF\cdot5H_2O$	Ligand	NFZ	DMF	1.04×10^5	75 ppb	55
	Ligand	NFT	DMF	7.19×10^4	131 ppb	
	Ligand	FZD	DMF	6.38×10^4	143 ppb	
$[Cd_2(L)(BPDC)_2]\cdot DMF\cdot9H_2O$	Ligand	NFZ	DMF	1.33×10^5	60 ppb	55
	Ligand	NFT	DMF	6.93×10^4	142 ppb	
	Ligand	FZD	DMF	5.4×10^4	170 ppb	
$Co(S\text{-}Hcna)_2$	Ligand	NFT	DMF	2.51×10^4	313 ppb	56
	Ligand	NFZ	DMF	2.25×10^4	290 ppb	
	Ligand	FZD	DMF	2.88×10^4	227 ppb	
$Cd_2((1S,2S)\text{-}Hcpba)_2(phen)_2$	Ligand	NFT	DMF	2.43×10^4	353 ppb	56
	Ligand	NFZ	DMF	2.21×10^4	322 ppb	
	Ligand	FZD	DMF	1.55×10^4	461 ppb	
	Ligand	MDZ	DMF	1.76×10^4	350 ppb	
	Ligand	DTZ	DMF	2.17×10^4	233 ppb	
$[Zn(L)]\cdot CH_3CN$	Ligand	DTZ	DMF	6.61×10^5	1.35 ppm	57
	Ligand	SDZ	DMF	7.18×10^2	1892 ppm	
	Ligand	NFZ	DMF	2.41×10^6	0.62 ppm	
	Ligand	NFT	DMF	2.48×10^6	0.78 ppm	
	Ligand	FZD	DMF	2.91×10^5	6.87 ppm	
$[Zn(L)(phen)]\cdot0.5DMF$	Ligand	NFT	DMF	1.27×10^4	6.7 μM	58
	Ligand	NFZ	DMF	1.45×10^4	5.4 μM	
$[Zn_2(L)_2(4,4'\text{-}bipy)]\cdot4DMF$	Ligand	NFT	DMF	1.30×10^4	2.0 μM	58
	Ligand	NFZ	DMF	1.14×10^4	2.5 μM	
$[Cd_2(L)(bpda)_2]\cdot3DMF\cdot H_2O$	Ligand	NFZ	DMF	3.11×10^4	252 ppb	59
	Ligand	NFT	DMF	2.20×10^4	465 ppb	
	Ligand	FZD	DMF	1.08×10^4	969 ppb	
$[Zn(TIPA)pim_{0.5}]2H_2O\cdot NO_3$	Ligand	OFX	DMF	4.61×10^4	—	60
$[Zn_2(BIP)_2(L)]\cdot2H_2O$	Ligand	NFT	DMF	1.59×10^4	37.5 μM	61
$[Zn_2(TRZ)_2(DBTDC\text{-}O_2)]\cdot DMAc$	Ligand	NFZ	DMF	5.2×10^4	0.404 μM	62
	Ligand	NFT	DMF	1.8×10^5	0.353 μM	
$[Cd_3(DBPT)_2(H_2O)_4]\cdot5H_2O$	Ligand	ONZ	Water	2.4×10^4	5 μM	63
	Ligand	MDZ	Water	2.0×10^4	10 μM	
	Ligand	DMZ	Water	1.7×10^4	10 μM	
	Ligand	2-M-5-MZ	Water	1.1×10^4	10 μM	
$[Zn(ACA)_4]\cdot CB[6]\cdot[NH_2(CH_3)_2]\cdot8H_2O$	Ligand	PAL	Water	5.74×10^4	0.34 μM	64
	Ligand	BER	Water	4.2×10^4	0.34 μM	
$[Na_4CB[6](H_2O)_{12}]\cdot2BPDS_2\cdot4H_2O$	Ligand	LUX	Water	6.47×10^4	0.16 μM	65
	Ligand	GAT	Water	9.1×10^4	0.11 μM	
BUT-172	Ligand	NOR	Water	6.0×10^4	0.18 μM	66
	Ligand	ENR	Water	5.0×10^4	0.22 μM	
	Ligand	CIP	Water	5.07×10^4	0.22 μM	
$Cd_4(L)_4\cdot H_2O\cdot EtOH$	Ligand	NFT	Water	1.9×10^4	10.3 μM	67
$Zn_2(oba)_4(4,4'\text{-}bpy)_2$	Ligand	MDZ	Water	6.44×10^3	0.81 mg L^{-1}	68
$[Cd_2Cl(L)(H_2O)]\cdot11H_2O$	Ligand	NFZ	Water	2.1×10^4	0.2 μM	69
	Ligand	NFT	Water	1.5×10^4	0.26 μM	
$Zn(oba)_2(bpy)_2$	Ligand	SMZ	Water	1.125×10^4	1.02 μM	70
$[Me_2NH_2][In(L)]\cdot2.5NMF\cdot4H_2O$	Ligand	NFZ	Water	3.35×10^4	0.55 mM	71
$[Mg_2(APDA)_2(H_2O)_3]\cdot5DMA\cdot5H_2O$	Ligand	NFZ	Water	9.0×10^4	108 ppb	72
	Ligand	NFT	Water	8.82×10^4	126 ppb	
$[Zn_2(Py_2TTz)_2(BDC)_2]\cdot2(DMF)\cdot0.5(H_2O)$	Ligand	NFZ	Water	1.73×10^4	0.91 μM	73
$[Cd_2(Py_2TTz)_2(BDC)_2]\cdot2(DMF)$	Ligand	NFZ	Water	4.54×10^4	0.85 μM	
$\{[Zn_3(\mu_3\text{-}OH)(HL)L(H_2O)_3]\cdot H_2O\}$	Ligand	SQX	Water	3.7×10^4	0.91 μM	74
	Ligand	STZ	Water	2.2×10^4	0.85 μM	
$Na_2(DCPB)\cdot(H_2O)_2$	Ligand	NFZ	Water	2.7×10^4	—	75
$Zn_4O(BCTPE)_3$	Ligand	NFZ	Water	—	0.1 ppm	78
	Ligand	MDZ	Water	—	0.6 ppm	

This journal is © the Partner Organisations 2020

Inorg. Chem. Front., 2020, **7**, 4293–4319 | **4295**

Table 1 (Contd.)

MOF	Luminescence source	Analyte	Media	K_{sv} (M^{-1})	LOD	Ref.
PCN-128Y	Ligand	TC	Water	9.84×10^5	30 nM	79
[Cd$_7$(SO$_4$)$_6$(tppe)$_2$](2DMF·2H$_2$O)	Ligand	FZD	Water	7.4×10^4	—	80
	Ligand	NFZ	Water	1.74×10^3	—	
	Ligand	ODZ	Water	7.56×10^2	—	
Cu$_4$I$_4$(EBT)$_5$	Cu$_4$I$_4$	TCH	Water	3.8×10^2	4.8 ppm	84
Cu$_4$I$_4$(ETBT)$_4$	Cu$_4$I$_4$	TCH	Water	3.23×10^3	4.15 μM	85
Eu$_2$(2,3′-oba)$_3$(phen)$_2$	Eu	MDZ	Water	2.39×10^4	2.75 μM	91
Eu(BTB)DMF	Eu	SMZ	Water	4.598×10^4	0.6554 μM	92
[NaEu$_2$(TATAB)$_2$(DMF)$_3$]·OH	Eu	ODZ	Water	—	0.8 μM	93
[Eu(H$_2$O)(BTCTB)]·2H$_2$O	Eu	NFZ	Water	1.27×10^4	0.67 μM	94
	Eu	NFT	Water	2.1×10^4	0.6 μM	
	Eu	FZD	Water	1.72×10^4	0.51 μM	
[EuCd$_{1.5}$L$_2$(H$_2$O)$_3$]·2H$_2$O	Eu	RDZ	Water	1.506×10^4	1.859 μM	95
Eu$_2$(TDC)$_3$(CH$_3$OH)$_2$·(CH$_3$OH) (λ_{ex} = 368 nm)	Eu	ODZ	Water	1.28×10^5	0.319 μM	96
	Eu	RDZ	Water	1.17×10^5	0.51 μM	
Eu$_2$(TDC)$_3$(CH$_3$OH)$_2$·(CH$_3$OH) (λ_{ex} = 385 nm)	Eu	ODZ	Water	1.97×10^5	0.183 μM	
	Eu	RDZ	Water	2.12×10^5	0.141 μM	
(Tb(TATMA)(H$_2$O)·2H$_2$O)	Tb	NFT	Water	3.35×10^4	—	97
	Tb	NFZ	Water	3×10^4	—	
[TbZn$_3$(L)$_3$(HCOO)(H$_2$O)$_2$]·5H$_2$O	Tb	FZD	Water	1.151×10^6	49 ppb	98
	Tb	NFZ	Water	1.83×10^6	39 ppb	
	Tb	NFT	Water	9.25×10^5	52 ppb	
[Tb(TCPB)(DMF)]·dioxane·0.5H$_2$O (496 nm)	Tb	NFZ	Water	3.7×10^4	0.15 μM	99
	Tb	NFT	Water	3.6×10^4	0.071 μM	
[Tb(TCPB)(DMF)]·dioxane·0.5H$_2$O (551 nm)	Tb	NFZ	Water	3.1×10^4	0.13 μM	
	Tb	NFT	Water	2.4×10^4	0.18 μM	
[Tb(TCPB)(DMF)]·dioxane·0.5H$_2$O (591 nm)	Tb	NFZ	Water	3.7×10^4	0.082 μM	
	Tb	NFT	Water	2.1×10^4	0.14 μM	
[Tb(TCPB)(DMF)]·dioxane·0.5H$_2$O (626 nm)	Tb	NFZ	Water	3.1×10^4	0.055 μM	
	Tb	NFT	Water	1.7×10^4	0.12 μM	
TbL·2H$_2$O	Tb	NFT	Water	5.26×10^4	3.47 μM	100
[Tb(TATAB)(H$_2$O)]·2H$_2$O	Tb	DTZ	Water	3.42×10^4	0.0808 μM	101
	Tb	ODZ	Water	1.62×10^4	0.171 μM	
	Tb	MDZ	Water	2.23×10^4	0.124 μM	
	Tb	RDZ	Water	5.25×10^4	0.0527 μM	
[Tb(H$_2$O)(BTCTB)]·2H$_2$O	Tb	MDZ	Water	1.59×10^4	2.4 μM	102
	Tb	DTZ	Water	1.62×10^4	2.9 μM	
Dy(TCPB)(DMF)$_3$	Dy and ligand	NFZ	Water	—	0.0476 μM	103
	Dy and ligand	FZD	Water	—	0.0482 μM	
(H$_2$bpy)$_{0.5}$·[(UO$_2$)$_{1.5}$(ipa)$_2$(H$_2$O)]	U	THC	Water	4.1×10^4	0.82 ppm	107
[Zn(2,5-PDC)(H$_2$O)$_2$]·H$_2$O/Tb^{3+}	Tb	CFX	Water	1.1×10^5	72 ppb	111
MOF-76(Eu$_{0.04}$Tb$_{0.96}$)	Tb and Eu	MDZ	Water	2.95×10^4	18.3 ppb	112
	Tb and Eu	DTZ	Water	2.46×10^4	21.9 ppb	
	Ligand	NFX	Water	1.34×10^5	4.03 ppb	
	Ligand	CPFX	Water	8.82×10^5	612 ppt	
	Eu	NFT	Water	9.29×10^3	58.1 ppb	
	Eu	NFZ	Water	2.35×10^4	23 ppb	
RhB@ZIF-8	RhB	NFZ	Water	7.3×10^4	0.26 μM	113
	RhB	NFT	Water	1.8×10^4	0.47 μM	
	RhB	TC	Water	8.6×10^4	0.11 μM	
	RhB	OTC	Water	7.6×10^4	0.14 μM	
FSS@ZIF-8	FSS	NFZ	Water	8.0×10^4	0.31 μM	
	FSS	NFT	Water	2.0×10^4	0.35 μM	
	FSS	TC	Water	4.6×10^4	0.17 μM	
	FSS	OTC	Water	5.5×10^4	0.16 μM	
DEASM@Cd(cpon)·2H$_2$O	Ligand and DEASM	NFZ	Water	6.09×10^3	0.208 μM	114
HPTS@[Zn(TIPA)(NO$_3^-$)$_2$(H$_2$O)]·5H$_2$O	HPTS	NFZ	Water	1.72×10^4	—	115
	HPTS	NFT	Water	1.01×10^4	—	
	HPTS	FZD	Water	1.72×10^4	—	
TMPyPE@bio-MOF-1	TMPyPE	NFZ	Water	4.48×10^4	0.11 ppm	116
	TMPyPE	NFT	Water	4.42×10^4	0.134 ppm	
RhB@[Tb$_3$(dcpcpt)$_3$(HCOO)]·DMF·15H$_2$O	Ligand and RhB	NFZ	Water	5.98×10^4	99 ppb	117
	Ligand and RhB	NFT	Water	6.69×10^4	107 ppb	
	Ligand and RhB	CPFX	Water	1.67×10^4	716 ppb	
	Ligand and RhB	NFX	Water	5.71×10^4	201 ppb	
RhB-CDs@Cu$_2$L(OH$^-$)	Ligand and RhB-CDs	NFZ	Water	1.98×10^4	65 ppb	118
	Ligand and RhB-CDs	NFT	Water	2.09×10^4	74 ppb	
	Ligand and RhB-CDs	TC	Water	4×10^3	777 ppb	
	Ligand and RhB-CDs	NFX	Water	1.38×10^4	44 ppb	
	Ligand and RhB-CDs	CPFX	Water	2.5×10^4	25 ppb	

4296 | *Inorg. Chem. Front.*, 2020, **7**, 4293–4319

This journal is © the Partner Organisations 2020

Table 1 *(Contd.)*

MOF	Luminescence source	Analyte	Media	K_{sv} (M^{-1})	LOD	Ref.
MOG(Eu) xerogels	Eu	RDZ	Water	2.9×10^4	1.205 ppm	121
	Eu	ODZ	Water	2.1×10^3	0.542 ppm	
	Eu	MDZ	Water	2.3×10^4	0.999 ppm	
	Eu	DTZ	Water	1.4×10^4	0.377 ppm	
MOG(Tb) xerogel	Tb	SMZ	Water	8.0×10^4	0.086 ppm	122
	Tb	SDZ	Water	4.1×10^4	0.218 ppm	
Hydrogel [Eu$_2$(BPDC)(BDC)$_2$(H$_2$O)$_2$]$_n$	Eu	PCL	Water	6.352×10^3	7.65 μM	123
	Eu	PCL	Serum	6.726×10^3	8.74 μM	
[Eu$_2$(BCA)$_3$(H$_2$O)(DMF)$_3$]·0.5DMF·H$_2$O film	Eu	NFZ	Water	2.2×10^4	0.21 μM	124
	Eu	NFT	Water	1.6×10^4	0.16 μM	
Tb(HL)L(H$_2$O) test strips	Tb	OTC	Water	2.18×10^4	1.95 nM	125
	Tb	TC	Water	1.39×10^4	2.77 nM	
[Tb$_2$(AIP)$_2$(H$_2$O)$_{10}$]·(AIP)·4H$_2$O MMMs	Tb	NFZ	Water	2.8×10^4	0.35 μM	127
	Tb	NFT	Water	4×10^4	0.3 nM	
Eu$_2$(TDC)$_3$(CH$_3$OH)$_2$·(CH$_3$OH) MMM	Eu	MDZ	Water	2.81×10^4	0.34 μM	128
	Eu	DTZ	Water	2.61×10^4	0.51 μM	
[Tb(HIP)(H$_2$O)$_5$]·(H$_2$O)·(HIP)$_{0.5}$ PMMA	Tb	MDT	Water	5.25×10^4	0.21 μM	129

Antibiotics are abbreviated as: NFZ = nitrofurazone; THI = thiamphenicol; MDZ = metronidazole; FZD = furazolidone; DTZ = dinitrazole; SDZ = sulfadiazine; NFT = nitrofurantoin; OFX = ofloxacin; ONZ = ornidazole; DMZ = dimetridazole; 2-M-5-MZ = 2-methyl-5-nitroimidazole; PAL = palmatine; BER = berberine; LUX = levofloxacin, GAT = gatifloxacin; OFX = ofloxacin; NOR = norfloxacin; ENR = enrofloxacin; CIP = ciprofloxacin; SMZ = sulfametahazine; SQX = sulfaquinoxaline; STZ = sulfathiazole; TC = tetracycline; ODZ = ornidazole; TCH = tetracycline hydrochloride; RDZ = ronidazole; MDT = macrodantin; CFX = cefixime; CPFX = ciprofloxacin; NFX = norfloxacin; OTC = oxytetracycline; PCL = penicillamine.

phenomenon, indicating the significant role of these organic ligands in LMOFs. Meanwhile, functional groups in organic ligands not only change the electron transitions, but also affect the luminescence emission.

Notably, metal ions/clusters as connect nodes for organic ligands are able to participate in the luminescence emission *via* altering charge transitions. The commonly used metal cations in LMOFs based on luminescent organic ligands are mainly focused on unsaturated d-orbitals (*e.g.*, Hf^{4+} and Zr^{4+}) or fully filled d-electron orbitals (*e.g.*, Zn^{2+} and Cd^{2+}). There are some interactions in LMOFs to affect the luminescence property, such as ligand-to-metal charge transfer (LMCT), metal-to-ligand charge transfer (MLCT), and inter-ligand charge transfer (ILCT).[48]

2.1. Electronic-rich conjugated organic ligand-based LMOFs

So far, the most common kind of LMOFs has been successfully constructed by using various electronic-rich conjugated organic ligands. This is because they have strong luminescence signals by themselves. When such ligands are coordinated with transition metals, especially the outer saturated d-orbital, the resultant LMOFs emit the luminescence emission originating from the electronic-rich conjugated organic ligands. In general, Co(II), Ni(II), and Fe(II)/Fe(III) are not suitable to be employed as metal centres to assemble with these lumine-scence ligands to generate LMOFs. This is because these metal cations have obvious electron deficient orbitals and distinct colours to cause the luminescence disappearance in MOFs. Recently, some LMOFs based on electronic-rich conjugated luminescence ligands have been reported and implemented as probes for antibiotic detection (Table 1).[44,49–61]

In 2016, B. Wang and co-authors reported the first case of LMOF in the detection and removal of antibiotics in water.[44] Two predesigned electronic-rich conjugated ligands with

luminescence property, namely 5′-(4-carboxyphenyl)-2′,4′,6′-tri-methyl-[1,1′:3′,1″-terphenyl]-4,4″-dicarboxylic acid (H$_3$CTTA) and 6,6′,6″-(2,4,6-trimethylbenzene-1,3,5-triyl)tris(2-naphthoic acid) (H$_3$TTNA), were synthesized and further reacted with ZrCl$_4$ to form two isostructural luminescent Zr-MOFs based on the classical Zr$_6$ cluster (denoted as BUT-12 and BUT-13) (Fig. 1a). Both porous three-dimensional (3D) LMOFs have lots


Fig. 1 (a) Crystal structures of BUT-12 based on H$_3$CTTA and BUT-13 based on H$_3$TTNA. Emission spectra of (b, c) BUT-12 and (d, e) BUT-13 upon incremental addition of NFZ and THI. Reproduced from ref. 44 with permission from American Chemical Society.

This journal is © the Partner Organisations 2020

Inorg. Chem. Front., 2020, **7**, 4293–4319 | **4297**

of porosity with a Brunauer–Emmett–Teller (BET) surface area of 3387 and 3948 m^2 g^{-1}. Meanwhile, they showed high stability in water, NaOH aqueous solution (pH = 10), HCl aqueous solutions of 2 M, 6 M, and concentrated HCl, respectively. According to the excellent stability, porosity, and strong luminescence emission, they possessed outstanding absorption and detection performance of antibiotics in water. In this work, twelve familiar antibiotics of five classes as analytes were selected to estimate the detectability of both LMOFs toward these antibiotics. The luminescence spectra of LMOFs were derived from free ligands. For the sake of exploring the detection ability, the luminescence signal was collected in the antibiotic aqueous solution. An obvious luminescence quenching phenomena happened after immersion in the NFZ aqueous solution, but only a small decrease was observed in THI. As found in Fig. 1b–e, the emission intensities of BUT-12 and BUT-13 dispersed in water were gradually quenched with the incremental amounts of NFZ, and demonstrated small changes in THI aqueous solution. According to the Stern–Volmer equation, the quenching constant (K_{sv}) values of BUT-12 and BUT-13 were calculated as 3.1×10^5 and 7.5×10^4 M^{-1} for NFZ with the limit of detection (LOD) of 58 and 90 ppb, respectively. The luminescence quenching mechanism is not only attributed to PET, but also resonance energy transfer. However, it should be noted that the selectivity of both LMOFs still needs to be improved to realize practical applications. More attention should be focused on the design and synthesis of LMOFs with high specific selectivity by means of modified ligands, different pore sizes, or tunable metal clusters.

It is known that MOFs are long-range ordered crystalline materials and possess precise skeleton structures, which can be analysed well by a single crystal diffractometer. Meanwhile, both composition and structure can be subtly controlled and designed for enhancing the desired performance. Hence, it is of great significance in the exploration of the structure–function relationship between LMOFs and their sensing performance. Such research studies will be beneficial to the follow-up work to design more efficient LMOFs in the detection of targeted antibiotics. Nevertheless, most research studies are focused on the synthesis of unreported LMOFs and investigation of their sensing behaviours. To date, only few studies have focused on enhancing the sensing ability by adjusting the structures of LMOFs, including the functional group and interpenetration.[49,50]

In 2018, Hou *et al.* reported two In-based LMOFs as interpenetration-dependent probes for sensing NFZ in water, which is the only example to investigate the skeleton interpenetration-dependent sensing performance toward the antibiotic NFZ.[49] As displayed in Fig. 2a, a conjugated organic ligand, 5-(2,6-bis (4-carboxyphenyl) pyridin-4-yl) isophthalic acid (H$_4$BCP), was synthesized and reacted with In(NO$_3$)$_3$ to generate two entirely different structures by rationally regulating the reaction solvents. A 3D anionic framework, namely V101, was generated in *N,N*-dimethylformamide (DMF), which is a 2-fold interpenetration framework with (4,4)-connected *sqc*-type topology. On the other hand, another novel robust non-interpenetration struc-
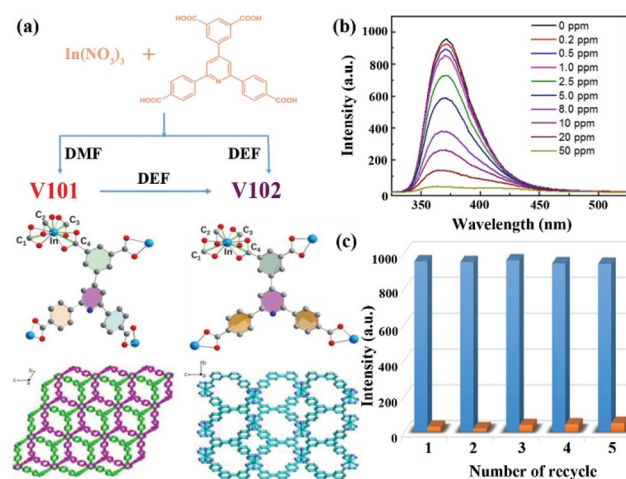
Fig. 2 (a) Crystal structures of both In-based MOFs. (b) The luminescence emission spectra of V102 in the NFZ aqueous solution at different concentrations. (c) The recyclability of V102 toward NFZ. Reproduced from ref. 49 with permission from American Chemical Society.

ture, namely V102, was constructed after changing DMF to *N,N*-diethylformamide (DEF). The PXRD patterns imply that V101 can keep the crystal structure in water and aqueous solutions in a wide pH range of 2–12, and V102 is still stable in water and aqueous solutions in a pH range from 4 to 9 at room temperature. Both In-based LMOFs showed a broad luminescence emission at 372 nm derived from the π → π* transition of H$_4$BCP. Thanks to the high luminescence emission and water stability, they are used as indicators to monitor antibiotics in water. There is a negligible influence on the luminescence emission of V101 in the detection of these selected antibiotics, but a significant quenching phenomenon of V102 can be found in the NFZ aqueous solution. The gigantic divergence may be caused by different pore sizes depending on the interpenetration-dependent structures. The NFZ size is about 7.7×11.8 Å^2, which can freely enter the larger channel size of 9.5 Å in V102 and is unable to get into the smaller pore size of 6.8 Å in V101. This assumption is proved by the NZF adsorption behaviour of both LMOFs. According to the UV–Vis absorption spectra, only V102 can gradually absorb NFZ in water with increasing immersion time. The quenching performance of V102 was found after immersion in a NFZ aqueous solution at 0.2 ppm (Fig. 2b). Additionally, the emission intensity continuously decreased at the higher NFZ concentration, and almost completely quenched at 50 ppm. The K_{sv} value was calculated to be 6.38×10^4 M^{-1} for NFZ. V102 had excellent recyclability even after reusing five cycles due to the high water stability as a solid material (Fig. 2c). The PXRD pattern of the reused samples kept the characteristic peaks of the original samples. Meanwhile, no In(III) cation was detected in the solution after centrifugation by inductively coupled plasma mass spectrometer (ICP-MS). Both results strongly proved the stability of V102 during the sensing process. The quenching behaviour was not triggered by the

4298 | *Inorg. Chem. Front.*, 2020, **7**, 4293–4319

This journal is © the Partner Organisations 2020

skeleton collapse. The Stern–Volmer equation showed a distinct deviation from linearity and became warped in the higher concentration range because of the coexistence of dynamic and static quenching processes. This work provides an effective approach to enhance the luminescence detectability by preparing large porous LMOFs. Pores in the host LMOFs are an important influencing factor for monitoring antibiotics. Hence, the reasonable design and regulation of the porous environments should be taken into consideration for the luminescence detection performance.

In addition, Zhou *et al.* prepared three isostructural Zn-based LMOFs with remarkable water stability by the mixed ligand strategy of carboxylic acid- and pyridine-based organic ligands.[50] The functional substituents, electron-donating group of –NH$_2$, neutral H, and electron-withdrawing –COOH group were rationally designed and decorated in the one-dimensional (1D) channels of porous LMOFs *via* crystal engineering. Three LMOFs are Zn(L)(aip)·(H$_2$O) (LMOF–NH$_2$), Zn(L)(ip)·(DMF)(H$_2$O)$_{1.5}$ (LMOF) and Zn(HBTC)(L)·(H$_2$O)$_2$ (LMOF–COOH) (H$_2$aip = 5-aminoisophthalic acid, Hip = isophthalic acid, H$_3$BTC = 1,3,5-benzenetricarboxylic acid, L = N4,N4′-di(pyridine-4-yl)biphenyl-4,4′-dicarboxamide). These samples have remarkable luminescence emission from organic ligands, which served as indicators to monitor antibiotics. For the same antibiotic, the sensitivity order is LMOF–NH$_2$ > LMOF > LMOF–COOH. This is because the electron-deficient –COOH group favors the π electron transfer from LMOF to the electron-withdrawing antibiotics, whereas the electron-donating –NH$_2$ can impede this process and reduce the energy level matched-degree between LMOFs and antibiotics. From this work, it is clearly shown that the functional groups in LMOFs have a certain influence on antibiotic detection. However, this result should be further analyzed and confirmed by theoretical calculation. This is because the introduced functional groups change the highest occupied molecular orbital (HOMO) and lowest unoccupied molecular orbital (LUMO) energy levels of the ligands, and generate various interaction forces between the antibiotics and LMOFs (*e.g.*, hydrogen bond, π–π force, and electrostatic interaction) to affect the luminescence sensing ability.

Some other similar LMOFs have been reported to detect antibiotics by luminescence quenching performance. However, most LMOFs are not stable in water or non-porous structures, leading to the detection process in organic solvents and poor sensing ability.[51–61] For example, some LMOFs, such as [(Zn$_4$O)$_2$(PDDA)$_6$(H$_2$O)$_2$]·10DMF (H$_2$PDDA = 4,4′-(pyridine-2,6-diyl) dibenzoic acid),[51] [Cd$_4$K$_4$(TADA)$_4$(H$_2$O)$_{12}$]·6DMF (TADA = 3,3′-((6-hydroxy-1,3,5-triazine-2,4-diyl)bis(azanediyl)) dibenzoate),[52] [NH$_2$(CH$_3$)$_2$]$_4$[Zn$_3$(HBDPO)$_2$(SO$_4$)$_2$] (H$_4$BDPO = 2,4-bis(3,5-dicarboxyphenylamino)-6-ol triazine),[53] [Cd$_3$(TDCPB)·2DMAc]·DMAc·4H$_2$O (H$_6$TDCPB = 1,3,5-tris[3,5-bis(3-carboxyphenyl-1-yl)phenyl-1-yl]benzene),[54] are not stable in water to make the luminescence sensing process in DMF. The deficiency directly restricts the practical application of LMOFs. Thus, the design and synthesis of high porous LMOFs with excellent water stability is still urgent to realize the sensi-

tive detection performance in water and other water environments. Recently, some water-stable LMOFs based on luminescent organic ligands were prepared for antibiotics detection.[62–75] For instance, a highly stable pillar-layer Zn-based LMOF, [Zn$_2$(TRZ)$_2$(DBTDC-O$_2$)]·DMAc (H$_2$DBTDC-O$_2$ = S,S-dioxodibenzothiophen-3,7-dicarboxylic acid, HTRZ = 1,2,4-triazole, and DMAc = N,N-dimethylacetamide) was prepared by using hard–soft-acid–base (HSAB) and dual-ligand strategies, which has the water stability and luminescence emission.[62] The corresponding K_{sv} values for NFZ and NFT were 5.2 × 10^4 and 1.8 × 10^5 M^{-1} with the LOD of 4.04 × 10^{-7} and 3.53 × 10^{-7} M, respectively. Table 1 summarizes all reported LMOFs for monitoring antibiotics.

2.2. Highly luminous tetraphenyl ethylene-based LMOFs

Tetraphenyl ethylene possesses an aggregation-induced emission (AIE) behaviour with strong luminescence emission. Meanwhile, it can be easily decorated with various functional groups and preserves its luminescence property.[76] As a result, tetraphenyl ethylene-based organic ligands with coordination functional groups, such as carboxylic acid and pyridine, are excellent candidates to prepare LMOFs as sensing probes. In order to retain the luminescence property of the ligands, Zn(II) and Cd(II) metal cations were both used as metal nodes to coordinate with organic ligands to construct LMOFs. In particular, the Zr(IV) metal cation is also a good candidate to assemble with tetraphenyl ethylene-based organic ligands by reason of the multiple connection nodes of the Zr$_6$ clusters with carboxyl ligands contributing to the construction of highly stable MOFs.[77]

Up to now, three highly luminous tetraphenyl ethylene-based LMOFs have been synthesized and employed in the detection of antibiotics.[78–80] X.-G. Liu *et al.* synthesized a dicarboxyl-substituted tetraphenylethene (TPE) ligand, namely 4,4′-(1,2-diphenylethene-1,2-diyl)dibenzoic acid (H$_2$BCTPE), which was employed to assemble with Zn$_4$O(CO$_2$)$_6$ nodes to construct a two-fold 3D interpenetrated LMOF as [Zn$_4$O(BCTPE)$_3$] (Fig. 3a–c).[78] Due to Zn(II) with 3d^{10} outmost orbiting electron, the emission spectrum of this LMOF mainly stems from the free isolated ligands with the π → π* electron transition of the conjugated skeleton. A slight blue-shift emission was found in this LMOF because the fixed structure
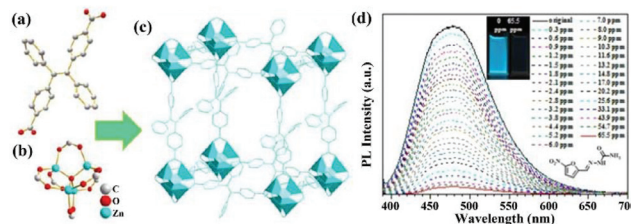
Fig. 3 (a) The BCTPE^{2-} ligand, (b) the Zn$_4$O(CO$_2$)$_6$ cluster in (c) the 3D structure. (d) Luminescence titration of this LMOF in aqueous solution at various NFZ concentrations. Inset: the optical photos at 0 and 65.5 ppm (NFZ). Reproduced from ref. 78 with permission from The Royal Society of Chemistry.

This journal is © the Partner Organisations 2020

Inorg. Chem. Front., 2020, **7**, 4293–4319 | **4299**

decreased the reorganization energy. The resultant micro-porous sample exhibited the luminescence emission with a high quantum yield of 64.5% and good water stability confirmed by PXRD patterns, which is the first case of using tetraphenyl ethylene-based MOFs for detecting nitro-containing antibiotics in aqueous conditions. The emission intensity of LMOF rapidly reduced by about 50% in the MDZ aqueous solution at a fixed concentration of 50 ppm, and 93% in NFZ at 50 ppm, illustrating that this sample can detect MDZ and NFZ by the quenching performance. For estimating the sensing ability of LMOF toward NFZ, the emission peak was collected at different concentrations by titrating tests, which began to wane after adding NFZ at 0.3 ppm and achieved full quenching of 97% at 65 ppm (Fig. 3d). Also, the calculated LOD was as low as 0.1 ppm, which is lower than 0.6 ppm for MDZ. Meanwhile, the water stability endows the preferable circularity by easy centrifugation and washing with water. In the purpose of understanding the detection mechanism, the HOMO and LUMO energy levels of NFZ and H_2BCTPE were theoretically calculated and analysed. The LUMO of H_2BCTPE is about −1.94 eV, which is significantly higher than −2.65 eV of NFZ to result in the obvious luminescence quenching. Notably, the usual fluorescence resonance energy transfer (FRET) hardly took effect for monitoring NFZ due to the minimal overlap between the UV-Vis absorption spectrum of NFZ and the emission spectrum of this LMOF.

In another example, Y. Zhou and co-workers developed a strong luminescent Zr(IV)-based MOF (PCN-128Y) by the coordination assembly of the Zr_6 cluster and TPE-based ligand (H_4ETTC) (Fig. 4a).[79] The Zr_6 cluster in PCN-128Y endowed the excellent physicochemical stability, and H_4ETTC as a luminous source vested the evident luminescence property of PCN-128Y.

PCN-128Y inherited the luminescence property of free H_4ETTC with an ultra-high quantum yield of 85.2%. The emission spectrum can keep well in water (even in a broad pH range), proving the remarkable luminescence stability and good water/pH tolerance. Hence, PCN-128Y is considered as a good candidate in the luminescence detection of antibiotic TC in water system. An obvious luminescence quenching behaviour of PCN-128Y was observed in the TC aqueous solution (0.1 mM) by naked eye under the UV lamp (365 nm) to imply the sensing ability toward TC (Fig. 4b). According to the luminescence titration by gradually adding TC in the detectable system from 0 to 1 μM, the corresponding emission intensities decrease with the increasing concentration. The K_{sv} value was calculated through the Stern–Volmer equation, which is as high as 9.84×10^5 M^{-1} with the LOD of 30 nM. Meanwhile, PCN-128Y possessed the high selectivity and anti-interference ability toward TC even in the presence of other antibiotics. In this work, the sensing mechanism was further investigated in detail. Firstly, the energy transfer between TC and PCN-128Y was excluded completely because of n spectral overlap between the UV–vis absorption of TC and the emission band of PCN-128Y (Fig. 4c). Nevertheless, the UV–Vis absorption band of TC had plenty of overlap with the excitation of PCN-128Y, illustrating that TC might impede PCN-128Y from absorbing the excitation light to generate the luminescence quenching. Then, the calculated HOMO and LUMO energies demonstrated that H_4ETTC has a higher LUMO energy level of −3.06 eV than TC (−4.53 eV), which is in favor of the PET process from PCN-128Y to TC (Fig. 4d). Finally, PCN-128Y has plentiful pores of large sizes to absorb TC in the porous structure, thus enhancing the detecting ability. This work provides an effective synergistic strategy of both adsorption and PET for antibiotic detection using mesoporous LMOFs.

In 2019, Zhao et al. synthesized a tetraphenylethene derivative tetrasubstituted with pyridyl groups, tetrakis(4-pyridylphenyl)ethylene (tppe), which was assembled with $CdSO_4$ to obtain the MOF $[Cd_7(SO_4)_6(tppe)_2]\cdot(2DMF\cdot2H_2O)$.[80] Similar with other Cd-based LMOFs, this LMOF inherited the luminescence property of the free tppe ligand with a slight red shift (~20 nm) because of the configurational change of ligand caused by the coordination with Cd clusters. This as-synthesized LMOF exhibits a high quantum yield of 58.3% and excellent stability in water for one week, leading to its potential application as a luminescence indicator in water. Through analysing the relationship of the emission intensity and antibiotic concentration, the K_{sv} values of FZD, NFZ, and ODZ were calculated as 7.4×10^4, 1.74×10^3, and 7.56×10^2 M^{-1}, respectively. The excellent sensitivity and selectivity of this LMOF toward such nitro-antibiotics is mainly ascribed to the charge transfer from the electron-rich ligand to the electron-deficient analytes. The lower LUMO energy levels of the antibiotics enabled the acceleration of the charge transfer phenomenon, which was further confirmed by the LUMO values in the following order: ODZ > NFZ > FZD > other selected antibiotics. Also, the energy transfer was another quenching reason verified by the spectral overlap degree
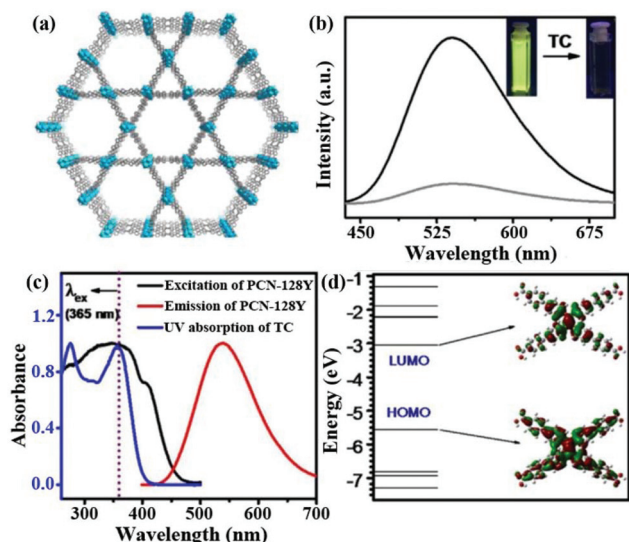

Fig. 4 (a) The 3D structure of PCN-128Y. (b) Emission spectra and inserted optical images of PCN-128Y with or without TC. (c) UV–Vis absorption spectrum of TC and excitation/emission spectra of PCN-128Y. (d) Calculated HOMO and LUMO of H_4ETTC. Reproduced from ref. 79 with permission from Elsevier.

between the UV–Vis adsorption spectra of the antibiotics and the emission peak of LMOF.

Based on the above luminous TPE-based LMOFs, it can be inferred that TPE derivatives are great candidates as bridging organic ligands to construct LMOFs with outstanding luminescence detection behaviour. However, only three cases have been reported up to now, which is not enough to analyse and summarize such LMOFs in the detection of antibiotics. It is urgent to design and prepare more LMOFs by the coordination assembly of various TPE-based ligands and different metal cations. More investigations should be focused on the relationship between the LMOF structures and their luminescence sensing behaviours, which is conducive to understanding how to prepare more efficient LMOFs for antibiotic detection.

3. LMOFs based on luminescent metal nodes

Another class of LMOFs can obtain the luminescence emission from metal nodes, such as transition metals and lanthanide metals. The luminescence property of most transition metal-based LMOFs originated from the organic ligand, along with the shift and alteration phenomenon of the emission peak. The luminescence behaviour of such LMOFs depended on the metal centres through the LMCT or MLCT processes. Notably, lanthanide metal cations matched well with the energy level of the organic ligands, resulting in an obvious antenna effect through the ligand-to-metal resonance energy transfer (LMREnT) process. Thus, the luminescence behaviour of lanthanide metal-based LMOFs primarily showed the characteristic peaks of the lanthanide cations. The distinct luminescence phenomena of LMOFs based on transition metal and lanthanide cations are mainly because of the following three factors of (1) spin–orbit coupling, (2) electronic repulsion, and (3) ligand field effect. Thus, the ligand field effect plays a more important role in the photophysical property in transition metal-based LMOFs than those based on lanthanide cations. This is because the ligand field perturbation of the d electron in the transition metal cations is evidently two orders of magnitude better than that of the f electron in the lanthanide cations. In addition, the electron shielding effect from the s and p electrons (located on the outside of the f electron) defends them from the ligands.

3.1. Copper iodide cluster-based LMOFs

The outermost electron is the d orbital in transition metals with the feasibility of LMCT or MLCT. The LMREnT process in transition metal-based MOFs can greatly attenuate the luminescence signal by reason of the non-radiative d–d transition. Thus, d^{10} metal cations of Zn(II) and Cd(II) without the non-radiative d–d transition are excellent candidates to construct LMOFs with the luminescence property from ligands, which has been discussed and analysed in the above section. For non-d^{10} transition metals as nodes in LMOFs, most of them have no luminescence emissions. The Cu(I) cation can coordi-

nate with the I-donor to generate various copper iodide clusters with nontoxic, low-cost, and photoactive properties, resulting in their potential applications in photophysics and photochemistry, such as light-emitting devices and responsive luminescent solid-state materials.[81,82] Meanwhile, copper iodide clusters are easily assembled with pyridine ligands or S-donor ligands to construct plentiful networks and various luminescence emissions.[83] Recently, two Cu_xI_y-based LMOFs have been reported as luminescence sensors for monitoring antibiotics.[84,85]

In 2018, G. Liu *et al.* synthesized a novel chair-like $[Cu_4I_4]$ cluster-based LMOF, $[Cu_4I_4(EBT)_5]$ (UJN-Cu, EBT = 3-ethyl-1,3-benzothiazole-2-thione) (Fig. 5a).[84] Due to the strong coordination bond between Cu(I) in Cu_4I_4 and the S-donor in the organic ligand, this LMOF has good water stability. In addition, this as-synthesized sample has an obvious luminescence spectrum in the solid state with bright light by naked eyes under UV lamp. The luminescence quantum yield is 9% and the lifetime is 9.13 μs, which are both comparable with other reported cubane-like copper(I) iodide clusters.[86,87] According to the density of state and optical absorption, the emission peak is generated by the charge-transfer triplet excited state between the Cu_4I_4 clusters and organic ligands. The prepared samples were milled and further pressed into a tablet with a ~5 nm diameter for luminescence sensing tests. As illustrated in Fig. 5b, the maximum quenching efficiency of UJN-Cu was found in the TCH aqueous solution, which was significantly more sensitive toward TCH than the other selected antibiotics. Furthermore, the emission intensity of UJN-Cu toward TCH decreased gradually with the incremental amount of TCH in the detectable system (Fig. 5c). Fig. 5d shows a good linear relationship of I_0/I and TCH concentration in a wide range of 0.04–3 mM, which can be used to calculate
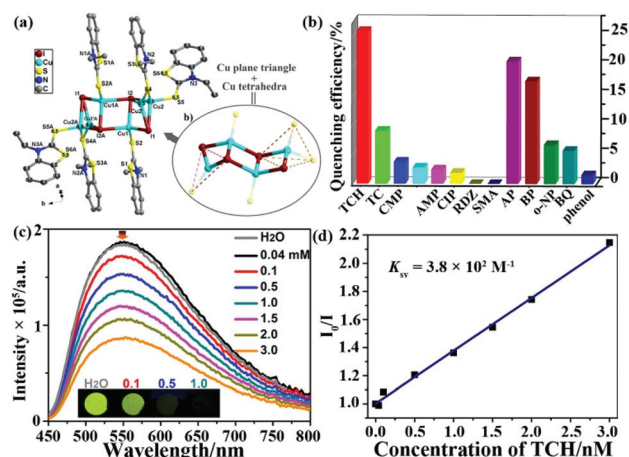
Fig. 5 (a) The chair-like $[Cu_4I_4]$ cluster and whole structure of UJN-Cu. (b) Quenching efficiencies of UJN-Cu toward different antibiotics. (c) Emission peaks of UJN-Cu in aqueous solutions with increasing TCH concentration. (d) The Stern−Volmer relationship of I_0/I and TCH concentration. Reproduced from ref. 84 with permission from the American Chemical Society.

This journal is © the Partner Organisations 2020

Inorg. Chem. Front., 2020, **7**, 4293–4319 | **4301**

the K_{sv} value of 3.8×10^2 M^{-1} with the LOD of ~4.8 ppm (10 μM). Meanwhile, UJN-Cu has good recyclability over five cycles and excellent selectivity toward TCH. The quenching mechanism was investigated by detecting the luminescence lifetime, which is similar with or without TCH to prove the static quenching effect rather than dynamic quenching effect. Meanwhile, the adsorption spectrum of TCH had a large overlap area with the excitation peak of LMOF, indicating the excitation light competition between UJN-Cu and TCH as the inner filter effect mechanism. This study represents the significance of the copper(I) iodine-based LMOFs as sensors for detecting antibiotics in water.

Soon afterwards, Liu and co-authors further reported a similar Cu₄I₄-based LMOF, [Cu₄I₄(ETBT)₄] (NJU-Cu2, ETBT = 2-ethylbenzo-[d]thiazole), which showed the luminescence emission and excellent water stability (Fig. 6a).[85] The lifetime of NJU-Cu2 centred at the emission peak of 578 nm was ~6.21 μs. This strong emission is ascribed to the charge transfer triplet excited state between Cu and the ligand, which is consistent with previous relevant mechanism studies of the copper iodine cluster.[84] From the sensing experiments, it was found that the prepared LMOF has the maximum luminescence quenching efficiency toward TCH with a quick response (Fig. 6b). The detectability of NJU-Cu2 toward TCH was evaluated by investigating the emission intensity and TCH concentration. As seen in Fig. 6c, the emission intensity of NJU-Cu2 was quenched little by little after enhancing the TCH concentration. The K_{sv} value is 3.23×10^3 M^{-1} with the LOD of 200 ppb (4.15 μM), according to the linear relationship of the Stern–Volmer plots of I_0/I and TCH concentration (Fig. 6d). The reusing tests of TCH detection proved that the sensing ability of UJN-Cu2 could be well preserved after at least five cycles. The possible luminescence quenching mechanism is the synergy of both static quenching effect and inner filter

Fig. 6 (a) The crystal structure of UJN-Cu2. (b) Quenching efficiencies of NJU-Cu2 toward different antibiotics. (c) Luminescence spectra of NJU-Cu2 in TCH aqueous solutions in the concentration range of 0–1.0 mM. (d) Stern–Volmer plots of UJN-Cu2 toward TCH. Reproduced from ref. 85 with permission from the American Chemical Society.

effect, which was similarly investigated as the previous UJN-Cu. Meanwhile, this LMOF possessed the selective recognition ability toward TCH from other interferent antibiotics.

However, only two Cu₄I₄-based LMOFs as luminescence probes have been reported to monitor TCH in aqueous solution. Hence, more LMOFs based on Cu$_x$I$_y$ clusters, such as Cu₂I₂ and Cu₈I₈, should be prepared for antibiotic detection through the luminescence signal response. Meanwhile, the exploration of copper iodide cluster-based LMOFs is still a challenge for monitoring other antibiotics besides TCH. Such issues require further exploration and discussion, but the Cu$_x$I$_y$-based LMOFs will acquire breakthroughs and exhibit more potential applications in the luminescence detection of antibiotics.

3.2. Ln(III) cation/cluster-based LMOFs

Among the metal cation/cluster-based LMOFs, the lanthanide-based luminescence emission is thought to be another vital part in LMOFs. Recently, various Ln(III)-based LMOFs have appeared in a large number of previous literature reports as optical devices and luminescence sensors.[88–90] Actually, lanthanides always have weak luminescence emission with extremely low quantum yield due to the forbidden f–f transition based on the principle of the Laporte selection rule. Fortunately, this difficult problem can be solved by introducing a sensitizer, which can absorb and transform the light energy to Ln(III). For the preparation of LMOFs, the organic ligands can be used as efficient sensitizers to enhance the luminescence intensity, which is called the "antenna effect". The transitions of lanthanides always happen from f-orbitals shielded by 5s- and 5p-orbitals to generate the undisturbed outer electronic environment of the f-orbitals, further resulting in sharp and narrow emission peaks in the Ln(III)-based LMOFs. Such LMOFs have been designed and employed as luminescence sensors for various antibiotics detection strategies. Recently, Li et al. synthesized a highly luminescent Eu(III)-MOF, [Eu₂(2,3′-oba)₃(phen)₂] (2,3′-H₂oba = 2,3′-oxybis(benzoic acid) and phen = 1,10-phenanthroline), with characteristic emission peaks at 581, 594, 616, 652 and 700 nm from the $^5D_0 \rightarrow {}^7F_J$ (J = 0–4) transitions.[91] The as-synthesized sample displayed a lifetime value of 1.068 ms for $^5D_0$ Eu(III) and a high quantum yield of 75.57%, illustrating that the aromatic ligand is an efficient Ln(III) sensitizer that offers an efficient energy transfer from the ligand to the Eu(III) centre. This Eu(III)-MOF exhibits different degrees of luminescence quenching toward antibiotics in water, especially for MDZ.

Furthermore, a more detailed study has been illustrated by Ren and co-authors.[92] A classical organic ligand, 1,3,5-tris(4-carboxyphenyl)benzene (H₃BTB), was selected in this work because this ligand not only has the large size to construct porous MOFs for guest molecule adsorption, but also possesses a conjugated π electron-donor to sensitize the Eu(III) cation. As shown in Fig. 7a and b, this ligand can coordinate with Eu(III) to generate a 2D LMOF [Eu(BTB)DMF] with 1D channels of 4 and 5 Å diameters. This Eu-MOF showed a bright red luminescence with four peaks from the $^5D_0 \rightarrow {}^7F_J$ (J
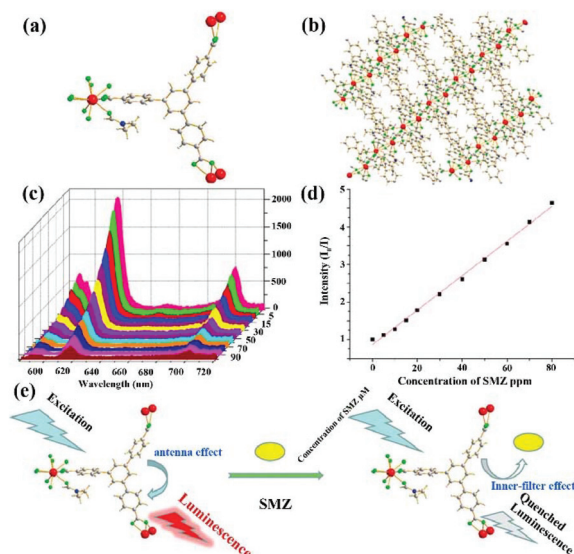
Fig. 7 (a, b) The structure of Eu-MOF. (c) Emission spectra of Eu-MOF at different SMZ concentrations. (d) Stern–Volmer plots of I_0/I and SMZ concentrations. (e) A possible mechanism of the inner filter effect for SMZ detection. Reproduced from ref. 92 with permission from the American Chemical Society.

= 1–4) transitions of Eu(III) under 287 nm. Meanwhile, the emission band of free H$_3$BTB disappeared in MOF, demonstrating the excellent "antenna effects" of this ligand as a sensitizer. This Eu-MOF possesses an evidently longer lifetime (τ = 725.5438 μs) than that of the free ligand (τ = 16.2751 ns) in solid state at room temperature. The emission peak of 614 nm originating from the $^5D_0 \rightarrow ^7F_2$ transition was selected as the response peak to study the sensing ability. Seven antibiotics were selected to investigate the luminescence emission of Eu-MOF, illustrating that a drastic quenching performance was found in the SMZ aqueous solution. Fig. 7c shows the emission peaks of Eu-MOF in water with different amounts of SMZ. The emission intensity evidently quenches with increasing SMZ concentration. As displayed in Fig. 7d, there is a good linear relationship with the R^2 value of 0.996 between the response signal values of I_0/I and the SMZ concentrations in the range of 0–80 μM. The obtained K_{sv} value is 4.598×10^4 M^{-1} with the LOD of 0.6554 μM at room temperature. The competition experiments prove the preferable selectivity toward SMZ. This Eu-MOF has excellent reusability after reusing five times due to its high stability. In this work, the authors investigated the probable quenching mechanism in detail. (1) The PXRD of the used samples can prove the skeleton integrity to eliminate the possibility of skeleton collapse as the quenching reason. (2) The increasing K_{sv} value at high temperature and the absence of the SMZ/MOF complex illustrate the dynamic quenching mechanism of the electron transformation from the MOF's conduction band to the LUMO of SMZ during the sensing process. (3) An obvious overlap between the UV-Vis absorption spectrum of SMZ and the absorption band of MOF declares that the inner filter effect is

another quenching mechanism in this sensing process (Fig. 7e). Some other Eu-based LMOFs were designed and utilized as luminescence indicators toward antibiotics by monitoring the characteristic peaks of Eu(III).[93–96]

Similar with the Eu-based LMOFs, the Tb cation is another commonly used lanthanide due to the bright-green luminescence of Tb-based MOFs, which served as sensors for monitoring analytes. Zhu *et al.* prepared a Tb-MOF, [Tb(TATMA)(H$_2$O)·2H$_2$O], by the coordination assembly of Tb(III) and 4,4′,4″-*s*-triazine-1,3,5-triyltri-*m*-aminobenzoate (H$_3$TATMA).[97] By virtue of the 1D Tb chains in this 3D MOF (Fig. 8a), it has extraordinary stability in most common organic solvents, air, and boiling water for one week. This sample exhibits the typical emission peaks of Tb(III) at 488, 544, 583, and 620 nm from the $^5D_4 \rightarrow ^7F_J$ (J = 6–3) transition. Furthermore, the disappeared emission peak of the ligand shows that TATMA^{3-} can sensitize the Tb(III) cations in this LMOF through the antenna effect. As illustrated in Fig. 8b, the maximum quenching effect of LMOF is observed in monitoring NFZ and NFT. The strongest luminescence peak at 544 nm is assigned to the magnetic-dipole-induced $^5D_4 \rightarrow ^7F_5$ transition, which emits green light and can be utilized as a responsive peak during the sensing process. Because of the good linear correlation of $[(I_0/I) - 1]$ *vs.* the NFZ or NFT concentrations (0–5 μM), the quenching constant of K_{sv} can be determined as 3.00×10^4 M^{-1} for NFZ and 3.35×10^4 M^{-1} for NFT, respectively (Fig. 8c and d). Due to the non-porous structure, fast responsive rate and high stability, the quenching mechanism was not caused by guest absorption and skeleton collapse. The UV-Vis result deduced that the probable quenching mechanism is attributed to the competitive absorption of the excitation light energy between MOF and antibiotic. More importantly, this LMOF can monitor NFT in practical bovine serum samples. Due to the high selectivity and recyclability, this Tb-MOF has the greatly promising application in the real antibiotic detection.
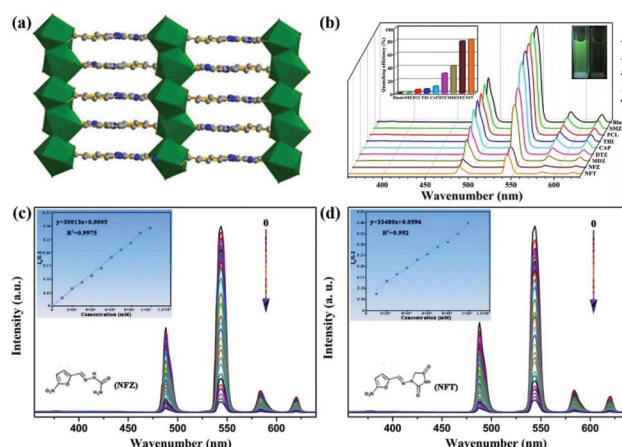
Fig. 8 (a) The 3D structure of Tb-MOF. (b) Emission spectra and optical images under UV lamp of Tb-MOF in different antibiotics. (c, d) Emission spectra of Tb-MOF and Stern–Volmer plots of $(I_0/I - 1)$ and NFZ or NFT concentrations. Reproduced from ref. 97 with permission from the American Chemical Society.

This journal is © the Partner Organisations 2020

Inorg. Chem. Front., 2020, **7**, 4293–4319 | **4303**

Another example has been reported by Zhou and co-authors. They used a terpyridyl-functionalized tricarboxylate organic ligand to react with the d/f metal cations of Zn(II) and Tb(III) to generate a new 3D heterometallic LMOF, [TbZn₃(L)₃(HCOO)(H₂O)₂]·5H₂O (namely CTGU-8) [H₃L = 4-(2,4,6-tricarboxyl phenyl)-2,2′:6′,2″-terpyridine].[98] As seen in Fig. 9a, the dinuclear $Tb_2(COO)_2$ cluster was generated by the Tb(III) and trimesic acid part, while this terpyridine can connect with Zn(II) to obtain a Zn_2L_2 unit. The d^{10} Zn(II) cation, f-metal Tb(III), and π-conjugated benzene ring are all present in CTGU-8, but the solid-state luminescence spectrum only shows four characteristic peaks from the transitions of $^5D_4 \rightarrow {}^7F_J$ (J = 6, 5, 4, and 3) from the Tb(III) cation by reason of the sensibilization of the π electron-rich ligand and Zn_2L_2. The quantum yield and lifetime of CTGU-8 in the solid state are estimated to be 4.19% and 1.56 μs at room temperature, respectively. The emission spectra have different intensities in various antibiotics, which showed the most obvious quenching efficiency for nitrofurans in all test antibiotics, including NFT, NFZ, and FZD (Fig. 9b). The corresponding K_{sv} values of CTGU-8 toward FZD, NFZ, and NFT are estimated to be 1.151 × 10⁶, 1.83 × 10⁶, and 9.25 × 10⁵ M⁻¹ with the LOD values of 49, 39, and 52 ppb for FZD, NFZ, NFT, respectively. The sensing mechanism accounts for the electron-transfer and inner-filter effect (IFE).

Most Tb-MOFs as luminescence sensors detect analytes *via* luminescence quenching, and evaluate the sensing ability by
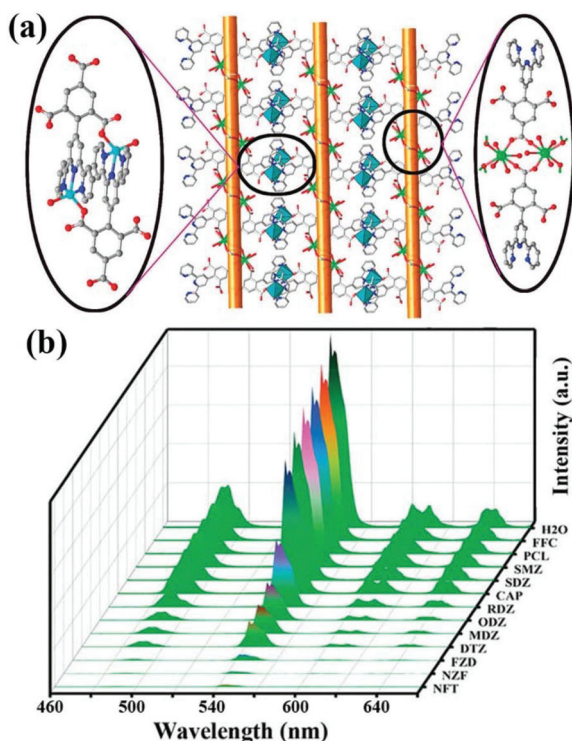

Fig. 9 (a) The structural of CTGU-8. (b) The emission spectra of CTGU-8 in different antibiotics aqueous solutions. Reproduced from ref. 98 with permission from the American Chemical Society.

using the strongest peak around 496 nm. In 2019, Zhang and co-authors prepared a LMOF, {[Tb(TCPB)(DMF)]·dioxane·0.5H₂O}ₙ, by using a flexible tripodal 1,3,5-tris(4-carbonylphenyloxy)benzene (H₃TCPB), which can monitor NFT and NFZ by luminescence quenching behaviour.[99] Notably, the K_{sv} values and LOD are obvious different by analysing the different emission peaks at 496, 551, 591, and 626 nm. In addition, some other Tb-based LMOFs have been employed as luminescence sensors in the detection of different antibiotics.[100–102] Eu- and Tb-MOFs have preferable detection effects with high sensitivity. However, the specificity of the sensing materials needs to be further improved for the targeted antibiotic because the luminescence quenching effect with different degrees can be observed for many antibiotics, especially for the same class of antibiotics. Meanwhile, the success or failure of the Eu(III) or Tb(III)-based LMOFs as the luminescence sensors toward antibiotics is mainly attributed to the same feature of the strong single absolute emission, which is easily affected by non-analyte factors. Notably, the ratiometric luminescence detection can overcome this limitation because this method has an inner reference signal to exclude most environmental interferences. Hence, this method can evidently increase the precision and selectivity for discerning different antibiotics even in real samples. The dual-emitting ratiometric Ln-based LMOFs are more promising sensing materials in the detection of antibiotics. The organic ligands with aromatic chromophores can be used to construct dual-emitting LMOFs, which not only can sensitize the luminescent emission of the Ln cations, but also can be considered as an excellent luminophor. However, the commonly used Eu(III) and Tb(III)-based LMOFs always only have the characteristic emission peaks of the Eu(III) and Tb(III) cations using organic ligands as sensitizing agents.

In a recent report, S. Wu and co-authors intelligently designed and prepared a water-stable 2D MOF, [Dy(TCPB)(DMF)₃]ₙ (H₃TCPB = 1,3,5-tris(1-(2-car-boxyphenyl)-1H-pyrazol-3-yl) benzene), which has two emission bands from the ligand and Dy(III).[103] This Dy-TCPB is a typical case for the fingerprint ratiometric luminescent indicator toward multiple antibiotics. Unlike LMOFs based on Eu(III) and Tb(III) metal cations, this Dy-TCPB not only has the characteristic luminescence peaks at 481 and 573 nm from $^4F_{9/2} \rightarrow {}^6H_{15/2}$ and $^4F_{9/2} \rightarrow {}^6H_{13/2}$, but also shows the broad emission band at 385 nm due to the incomplete energy transfer efficiency from the ligand to Dy(III) cation. Dy-TCPB with luminescence emission peaks of 385, 481, and 573 nm was used to detect various antibiotics in water by multi-dimensional ratiometric sensing. These luminescence signals were weak to varying degrees, especially for FZD and NFZ. A decoded map was cleverly delineated by assembling I_{385}/I_{481} and I_{385}/I_{573}, which provided the unique data point of each antibiotic to unambiguously distinguish between the different antibiotics. Because of the larger quenching effect of I_{385}/I_{573} than I_{385}/I_{481}, the concentration-dependent I_{385}/I_{573} was used as the ratiometric responsive signal for the antibiotics identification and detection. As displayed in Fig. 10a and b, the emission intensity of Dy-TCPB decreased as the concentration of FZD increased. This performance was still

4304 | *Inorg. Chem. Front.*, 2020, **7**, 4293–4319

This journal is © the Partner Organisations 2020

Fig. 10 (a) The emission intensity and (b) fitting curve of Dy-TCPB upon incremental addition of FZD. (c) The electron transfer from the LUMO of the ligand to the LUMO of NFZ or FZD. (d) The absorption band of H$_3$TCPB and NFZ/FZD. (e) The sensing mechanism of Dy-TCPB toward NFZ/FZD. Reproduced from ref. 103 with permission from Wiley-VCH.

observed in the NFZ aqueous solution. The ratio values of I_{385}/I_{573} showed the good linear relationship toward the NFZ and FZD concentrations, which illustrated that the calculated LOD values of NFZ and FZD were 0.0476 and 0.0482 μM, respectively. Meanwhile, the excellent water stability of Dy-TCPB endowed its outstanding reusability. The possible quenching mechanism is further discussed in detail. As observed in Fig. 10c–e, the mechanism may be attributed to the synergy effect of PET and photocompetitive absorption processes. This work provides a useful platform to selectively recognize different antibiotics from the decoded map. Hence, more attention should be focused on the construction of such LMOFs with multiple emission peaks as ratiometric responsive signals for analyte detection.

3.3. Uranyl-based LMOFs

Recently, uranyl LMOFs have been attracting lots of interest in the sensing field because of their unique luminescence characteristics.[104–106] First, they have a long lifetime for the time resolution, because the enhanced luminescence emission is derived from the triplet energy level of the ligand to uranyl ion. Then, the uranyl ion has an atomic level f–f transition to emit high purity luminescence signals with high resolution. In addition, the large Stokes shift is in favor of suppressing the interference. Finally, there is an obvious electron screening effect in the 5f electrons of the uranyl ion to reduce the exter-

nal interference of the f–f transition, resulting in the extremely stable luminescence emission.

So far, only one uranyl-based LMOF has been synthesized and utilized as a luminescence sensor in antibiotic detection.[107] An anion 2D layer of (H$_2$bpy)$_{0.5}$·[(UO$_2$)$_{1.5}$(ipa)$_2$(H$_2$O)] (H$_2$ipa = isophthalic acid, bpy = 4,4′-bipyridine) is generated by the crosslink between the UO$_2^{2+}$ units and isophthalate ligands, leading to the presence of the protonated bpy with negative charge as a balanced cation in the layers. The as-synthesized LMOF has five characteristic peaks at 464, 484, 503, 526, and 552 nm from the S$_{11}$ → S$_{00}$ and S$_{10}$ → S$_{0v}$ (v = 0–4) electron transport in the specific uranyl species. The strongest emission peak is located at 484 nm with a blue-shift of 24 nm compared to that of UO$_2$(NO$_3$)$_2$·6H$_2$O due to the coordination effect in LMOF. The as-synthesized U-MOF has significant luminescence quenching behaviour in the TCH aqueous solution. The luminescence intensity of U-MOF reduces bit by bit with the increased concentration of TCH in water. The I/I_0 based on the emission peak at 484 nm had a linear relationship with the TCH concentration under 40 ppm (Fig. 11a and b). The LOD of U-MOF toward THC was as low as 0.82 ppm, according to the detection limit formula. The calculated K_{sv} value was as high as 4.1 × 10^4 M^{-1}. The crystal structure was well preserved after reusing five cycles, implying the good recyclability. The HOMO and LUMO energies of these antibiotics were calculated by cyclic voltammetry. TCH possesses the lowest LUMO orbital level among these antibiotics, which is in agreement with the experimental results to prove the electron transfer theory as a quenching reason (Fig. 11c). This research presents that the uranyl-based LMOFs are preferable candidates for monitoring antibiotics. It is very urgent to prepare more LMOFs based on uranyl with higher lumine-
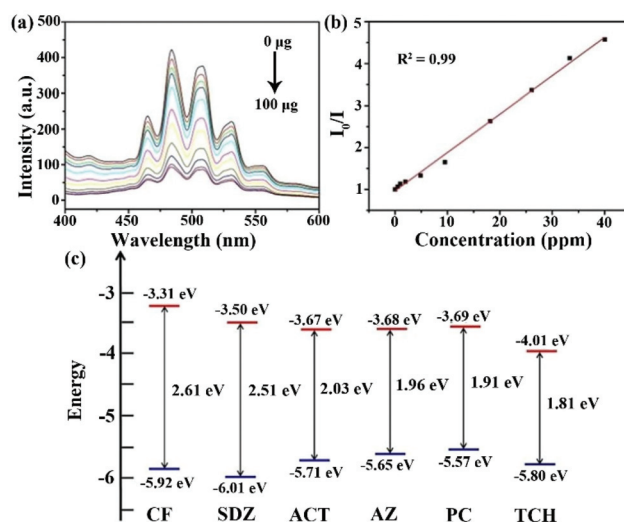
Fig. 11 (a) Emission spectra of U-MOF in the TCH aqueous solution with different TCH amounts, and (b) the corresponding Stern–Volmer plots. (c) HOMO and LUMO energies of these antibiotics calculated by cyclic voltammetry. Reproduced from ref. 107 with permission from Wiley-VCH.

This journal is © the Partner Organisations 2020

Inorg. Chem. Front., 2020, **7**, 4293–4319 | **4305**

scence intensity to realize a more sensitive and selective detection effect.

4. Ln(III)-Doped or adsorbed/linked lumophore-based LMOFs

Generally, MOFs always have plenty of uniform pore arrays and a controllable pore size, resulting in the feasibility of adsorbing luminescence light-emitting species as guests in the MOF host, including rare earth cations,[108] carbon dots,[109] and organic dyes.[110] The fabricated composites can realize the luminescence regulation and multiple emissions by integrating various luminescence components, leading to the outstanding sensing ability of the targeted analytes by the variation of the emission spectra and luminescence colours. This synthetic strategy is commonly used in the construction of LMOFs.

4.1. Ln(III)-Doped LMOFs

Ln(III) cations, especially Eu(III) with strong red luminescence and Tb(III) with green emission, are considered as commonly used luminescence species in MOFs, which have been fabricated and investigated as luminescence probes for antibiotic detection. One example was reported by Pan *et al.* in 2018.[111] They prepared a Tb^{3+}-doped Zn-based MOF of [Zn(2,5-PDC)(H$_2$O)$_2$]·H$_2$O (namely Zn-PDC/Tb^{3+}) *via* a straightforward solution precipitation method. The PXRD profiles and SEM images of Zn-PDC/Tb^{3+} and Zn-PDC have the same structure and shape. The more intuitive proof is that Zn-PDC/Tb^{3+} has four luminous peaks from the f–f electron transformation of the Tb^{3+} cation at room temperature with the outstanding stability in water. Thus, the strongest emission of 546 nm is generated from the $^5D_4 \rightarrow {}^7F_5$ transition as the responsive luminescence signal. As displayed in Fig. 12a, the emission intensity ratios of I_0/I showed the maximum value in the CFX aqueous solution. The sensing ability of Zn-PDC/Tb^{3+} was explored by analysing the relative luminescence intensity and CFX concentration, which shows the reduction of the luminescence emission at high concentrations. The green light disappeared at the CFX concentration of 13.33 μM under UV light (Fig. 12b). A fine linear relationship of $[(I_0/I) - 1]$ and CFX concentration can be seen in the low concentration range, but it is obviously nonlinear at high concentration due to the co-existence of static and dynamic quenching (Fig. 12c). The linear relation can be used to calculate the high K_{sv} value of 1.1×10^5 M^{-1} toward CFX. Meanwhile, the LOD is evaluated to be 72 ppb (0.14 μM). The quenching mechanism of Zn-PDC/Tb^{3+} toward CFX is primarily ascribed to the synergy of the electron transfer and IFE. In addition, the sensing ability can be well preserved for at least five cycles (Fig. 12d), proving the stability of this composite.

In 2020, Yang and co-authors reported another case of the integration of MOF-76 and the Eu^{3+} cation by easily exchanging the Eu^{3+} cation in MOF-76 (Fig. 13a).[112] It is well known that MOF-76 is a famous Ln-MOF with strong green lumine-
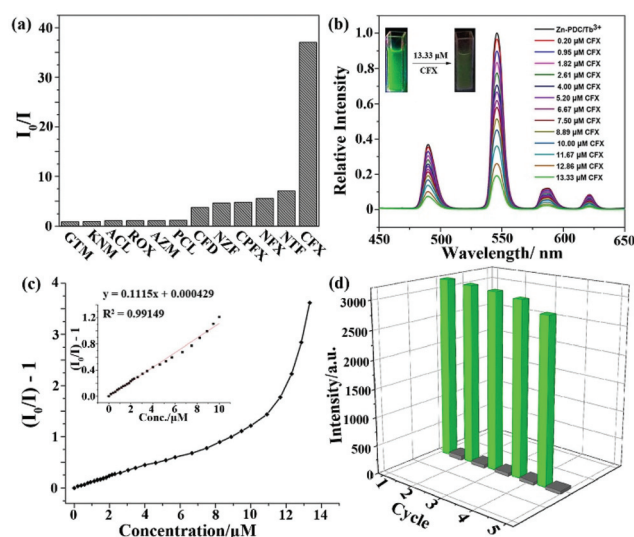

Fig. 12 (a) Luminescence quenching efficiencies of Zn-PDC/Tb^{3+} at 546 nm toward different antibiotics. (b) Emission peaks, (c) Stern–Volmer plots and (d) the reusability of Zn-PDC/Tb^{3+} toward CFX. Reproduced from ref. 111 with permission from the American Chemical Society.
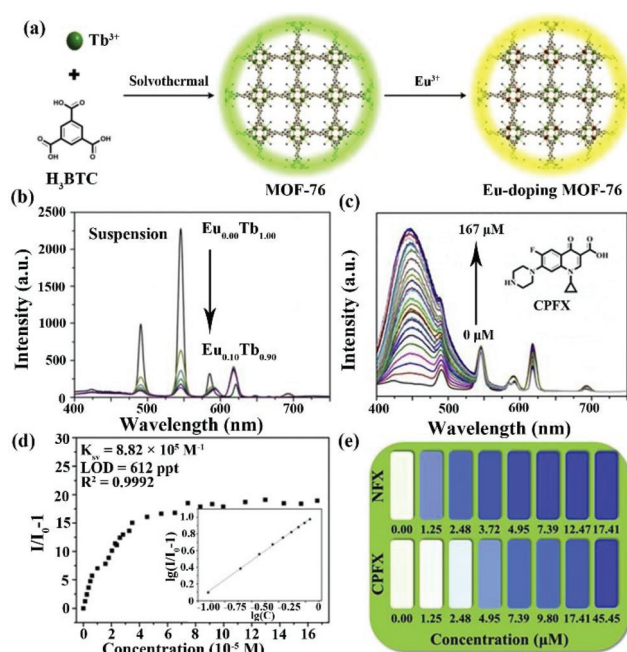

Fig. 13 (a) The preparation diagram of the Eu-doping MOF-76. (b) Luminescence emission of the Eu-doping MOF-76 with different Eu(III) amounts in water. (c) Concentration-dependent emission and (d) Stern–Volmer plots of MOF-76 (Eu$_{0.04}$Tb$_{0.96}$) toward CPFX. (e) The luminescence colour of MOF-76 (Eu$_{0.04}$Tb$_{0.96}$) at different NFX and CPFX concentrations. Reproduced from ref. 112 with permission from Elsevier.

scence, and is constructed by the Tb^{3+} cation and trimesic acid as sensitizer. Serious MOF-76(Eu$_x$Tb$_{1-x}$) (x = 0.02, 0.04, 0.06, 0.08 and 0.10) can be synthesized by tuning the added

4306 | *Inorg. Chem. Front.*, 2020, 7, 4293–4319

This journal is © the Partner Organisations 2020

amounts of Eu^{3+} cation. The PXRD profiles of Eu-doping MOF-76 prove that they have the same skeleton as MOF-76, and exhibit the excellent stability in water. Eu^{3+}-doping MOF-76 showed obviously visible emission peaks located at 590, 612, 649, and 698 nm of the Eu^{3+} cation because of the antenna effect and Tb-to-Eu energy transfer. As displayed in Fig. 13b, the emission intensity of Eu^{3+} increased significantly with increasing proportions of Eu^{3+} in MOF-76. Based on the 1931 Commision Internationale de L'Eclairage (CIE) chromaticity diagram, the MOF-76 ($Eu_{0.04}Tb_{0.96}$) suspension exhibited white light, which can be considered as a luminescence sensor toward antibiotics by the change of emission and colour. More interestingly, there are three distinct signal response modes in the detection of the three kinds of antibiotics. The luminescence signal of the lanthanide cations was implemented to monitor MDZ and DTZ. The quenching efficiencies were 2.95×10^4 M^{-1} for MDZ and 2.46×10^4 M^{-1} for DTZ with LOD values of 18.3 and 21.9 ppb (1.22 μM) for MDZ and DTZ, respectively. The sensing mechanism is the co-existence of energy transfer and competition of light absorption. For CPFX and NFX, the luminescence emissions of the lanthanide canters can keep well without obvious changes. However, the emission intensity in the range of 400–530 nm significantly increased with increasing CPFX and NFX concentration (Fig. 13c). Fig. 13d illustrates that the enhanced luminescent intensity was caused by static and dynamic processes. The K_{sv} values were 1.34×10^5 M^{-1} for NFX and 8.82×10^5 M^{-1} for CPFX. The LODs of NFX and CPFX were calculated to be as low as 4.03 ppb and 612 ppt. The colour of MOF-76($Eu_{0.04}Tb_{0.96}$) changed to blue at the concentration of 1.25×10^{-5} M (NFX) and 4.95×10^{-4} M (CPFX) (Fig. 13e). Finally, the luminescence emission of the ligand showed a bathochromic shift from 425 nm to 460 nm for detecting NFT and NFZ due to the guest absorption of both antibiotics. Meanwhile, the emission intensity of the Eu^{3+} cation at 612 nm as the responsive signal gradually weakened at high concentrations. The LODs values were estimated as 58.1 and 23.0 ppb for NFT and NFZ, respectively. The K_{sv} values of MOF-76($Eu_{0.04}Tb_{0.96}$) are 9.29×10^3 M^{-1} for NFT and 2.35×10^4 M^{-1} for NFZ. The various detection signals and luminescence colours of MOF-76(Eu_xTb_{1-x}) provide a feasible sensor to realize the highly sensitive detection of different antibiotics in water.

4.2. LMOFs with adsorbed or linked organic dyes

Guest organic dyes with strong luminescent emission are able to enter porous MOFs to fabricate host–guest composites by adsorption and ion exchange. By adjusting the disparate luminescence constitutes, single or multi-emitting luminescence sensors can be designed and prepared to offer more diversiform and precise information for monitoring target antibiotics. Notably, the obvious colour alteration may be observed during the sensing process and affected by different antibiotics.
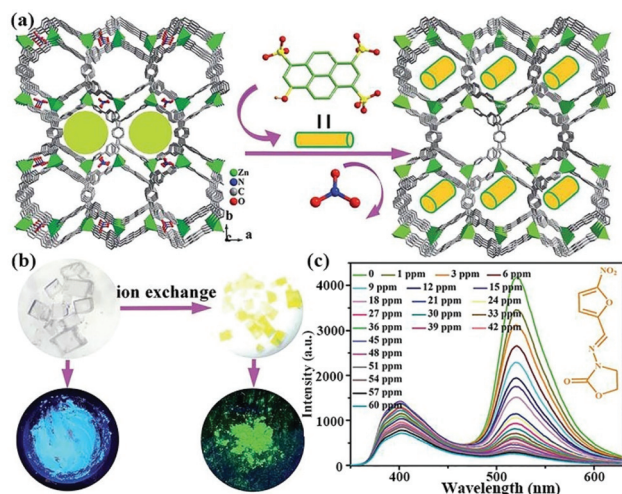
Zhang and co-authors in 2019 reported on two luminescent chemosensors by encapsulating rhodamine B (RhB) and fluorescein disodium salt (FSS) dyes as guest functional molecules into zeolitic imidazolate framework-8 (ZIF-8), namely RhB@ZIF-8 and FSS@ZIF-8.[113] Both composites had the same structure and shape as ZIF-8 to prove the stability during the fabrication process. Pure ZIF-8 has a wide luminescent band at 437 nm, but there were strong emission peaks located at 580 nm for RhB@ZIF-8 and 558 nm for FSS@ZIF-8 derived from the organic dyes. Thanks to the strong luminescence emission and water stability, both composites remarkably enhanced the super-sensitive detection capability toward nitrofurans and tetracyclines. The LOD values of RhB@ZIF-8 toward NFT, NFZ, TC, and OTC were 0.26, 0.47, 0.11, and 0.14 μM, respectively. The LOD of FSS@ZIF-8 were calculated to be 0.31, 0.35, 0.17, and 0.16 μM for NFT, NFZ, TC, OTC in water, respectively. The K_{sv} values of RhB@ZIF-8 were 7.3×10^4 M^{-1} for NFZ, 1.8×10^4 M^{-1} for NFT, 8.6×10^4 M^{-1} for TC, and 7.6×10^4 M^{-1} for OTC. The K_{sv} values of FSS@ZIF-8 toward NFT, NFZ, TC, and OTC were 8.0×10^4, 2.0×10^4, 4.6×10^4, and 5.5×10^4 M^{-1}, respectively. Moreover, FSS@ZIF-8 enabled monitoring NFT and TC in the real water system. The result manifested that the luminescence dye@MOF with single-emission favored detecting the antibiotics in water. Additionally, Xing and co-authors used a non-porous flexible MOF, Cd(cpon)·$2H_2O$, to encapsulate 4-(4-diethylaminostyryl)-1-methylpyridinium (DEASM) dye through the "pore-breathing effect".[114] The obtained composite is a dual-emission platform to detect NFZ in water. The corresponding quenching constant K_{sv} value is 6.09×10^3 M^{-1} with the LOD of 0.208 μM. The above results show the feasibility of the approach to construct functional LMOFs and their composites.

In 2018, Fu et al. prepared a 3D cation LMOF, [Zn(TIPA)(NO_3^-)$_2$(H_2O)]·$5H_2O$, by assembling tri(4-imidazolylphenyl) amine (TIPA) and Zn^{2+} under solvothermal conditions, which has high porosity and the NO_3^- anion as the counterion.[115] As displayed in Fig. 14a, 8-hydroxy-1,3,6-pyrenetrisulfonic acid (HPTS) is a typical anionic organic dye that was further imported into channels through the ion exchange method to fabricate a dual-emission luminescence composite. This composite has the same structure with the pristine MOF, but the optical images under natural light and UV lamp show the obvious colour change (Fig. 14b). The composite displays two emission bands in the range from 375 to 450 nm of MOF, and from 500 to 575 nm of HPTS. The emission intensity of this composite has the most obvious luminescence quenching phenomenon of 90% in NZF, FZT, and DTZ aqueous solutions at 60 ppm (Fig. 14c). On the basis of the luminescence titration tests, the relationship of the emission intensity and concentration is linear at low concentration. However, the other plots at high concentration are slightly bent. Based on the Stern–Volmer equation during the low concentration, the quenching constants are estimated to be 1.72×10^4 M^{-1} toward NFZ, 1.01×10^4 M^{-1} toward NFT, and 1.72×10^4 M^{-1} toward FZD. Therefore, this composite displays the outstanding response ability toward a wide range of nitro-antibiotics.

Ying and co-authors selected a 3D porous bio-MOF-1, which is a famous anion MOF, as a scaffold to encapsulate guest organic dyes.[116] As seen in Fig. 15a, the strongly lumi-

This journal is © the Partner Organisations 2020

Inorg. Chem. Front., 2020, **7**, 4293–4319 | **4307**

Fig. 14 (a) The fabrication process of importing HPTS into MOFs *via* ion exchange approach. (b) The natural optical and luminescent images of MOFs and composites. (c) Emission spectra of the composite toward NFZ at various concentrations at room temperature. Reproduced from ref. 115 with permission from The Royal Society of Chemistry.

Fig. 15 (a) Schematic diagram of the encapsulating luminescence of TMPyPE into bio-MOF-1. The colour change of (b) bio-MOF-1 and (c) TMPyPE@bio-MOF-1. Luminescence emission peaks of the activated composite toward (d) NFZ and (e) NFT with the incremental concentration at room temperature. Reproduced from ref. 116 with permission from The Royal Society of Chemistry.

nous tetrakis[4-(1-methylpyridin-4-yl)phenyl]ethene iodide (namely TMPyPE iodide) is a pyridine-substituted tetraphenylethene cation, which was selected and ingeniously introduced into bio-MOF-1 to fabricate the target composite TMPyPE@bio-MOF-1 by *in situ* synthesis. Although the structure of TMPyPE@bio-MOF-1 was consistent with that of bio-MOF-1, the corresponding colour of the composite had a sig-

nificant colour change from white to yellow (Fig. 15b and c). The activated composite was obtained by immersion in CH_2Cl_2. It was activated at 60 °C for 6–7 h under high vacuum, and was used as a luminescent sensing material to detect antibiotics in water. The luminesce emission of TMPyPE@bio-MOF-1 in the solid state showed a broad peak at 522 nm, but the emission peak of this activated composite exhibited a redshifted peak at 547 nm because of the enhancement of the electronic coupling between the guest TMPyPE cation and bio-MOF-1. The luminescence quantum yields were 78.5% of TMPyPE@bio-MOF-1 and 77.3% of the activated composite, respectively. By virtue of the high stability of bio-MOF-1, TMPyPE@bio-MOF-1 still possessed excellent stability in water. The activated TMPyPE@bio-MOF-1 was ground and dispersed in water as an indicator to monitor a variety of antibiotics. This sensing composite showed different levels of luminescence quenching behaviour. The most obvious quenching efficiencies of 96.0% and 95.5% were observed in NFZ and NFT aqueous solutions at a fixed concentration of 1 mM. The detection ability was evaluated by the luminescence titrations of NFZ and NFT in the detectable system. The emission intensity of activated TMPyPE@bio-MOF-1 decreased at high concentrations of antibiotics, accompanied by the disappearance of yellow colour. As illustrated in Fig. 15d and e, the K_{sv} values of NFZ and NFT were 4.48×10^4 and 4.42×10^4 M^{-1} with LOD values of 0.110 and 0.134 ppm, respectively. The energy competition of the excitation light and the decreased electron transfer are the dominant causes of luminescence quenching. For this work, only one emission peak was detected as the single responsive signal to reduce the anti-interference and accurate detection.

Yu and co-authors prepared an anionic 3D porous Ln-MOF, $[Me_2NH_2][Tb_3(dcpcpt)_3(HCOO)]\cdot DMF\cdot 15H_2O$ (denoted as Tb-dcpcpt), through the coordination assembly of $Tb(NO_3)_3\cdot 6H_2O$ and $H_3dcpcpt$ ($H_3dcpcpt$ = 3-(3,5-dicarboxylphenyl)-5-(4-carboxylphenl)-1H-1,2,4-triazole) under the solvothermal reaction.[117] The pink RhB@Tb-dcpcpt composite was successfully obtained by immersing Tb-dcpcpt into the RhB aqueous solution through cation exchange (Fig. 16a). The skeleton structure of RhB@Tb-dcpcpt showed almost no changes except for the guest cation, but they displayed an obvious colour change from white to pink under daylight, and from green to yellow under a UV lamp at 365 nm (Fig. 16b). The RhB@Tb-dcpcpt composite in the solid state had weak luminescence emission peaks from the Tb^{3+} cation and a strong emission band at 630 nm from RhB on the basis of the coexistence of FRET and PET. Generally, the water molecule not only easily breaks the structures of MOFs, but also reduces the luminescence emission intensity of the Ln(III) cations. Nevertheless, most pollutants need to be monitored in water, including drinking water, river, urine, and industrial waste water. Fortunately, this composite can preserve the luminescent behaviour with a slight reduction in water. Hence, both luminescence property and out-bound stability endowed the potential sensing ability toward antibiotics in aqueous solution. The luminescence emission spectra of the RhB@Tb-dcpcpt aqueous suspension
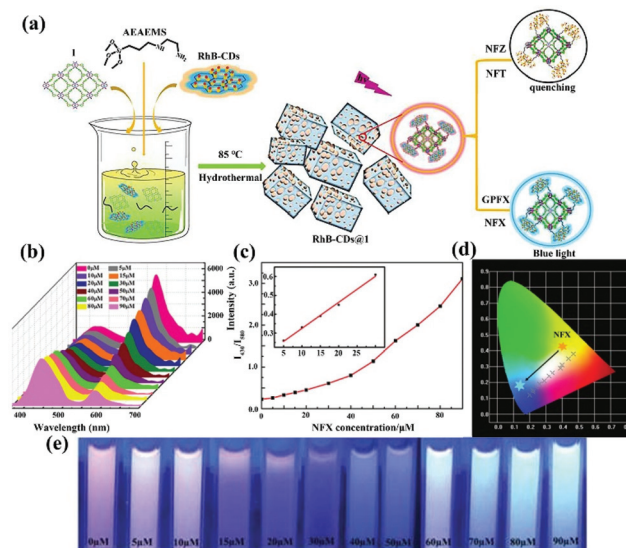
Fig. 16 (a) The 3D porous anion framework of Tb-dcpcpt and the fabrication of RhB@Tb-dcpcpt *via* cation exchange. (b) Photographs of both samples under natural light and UV lamp at 365 nm. Emission spectra of the RhB@Tb-dcpcpt aqueous suspension upon various concentrations of (c) NFX and (d) CPFX. (e) The corresponding luminescence colours. Reproduced from ref. 117 with permission from the American Chemical Society.

Fig. 17 Schematic illustration of fabricating the RhB-CDs@1 composite by post-synthetic modification for multi-component analysis. (b) Emission spectra of this composite in the NFX concentration (0–90 mM). (c) The relationship of the emission intensity ratio of (I_{430}/I_{580}) and NFX concentration. (d) CIE coordinates and (e) luminescent photographs under UV light of the composite in different NFX concentrations. Reproduced from ref. 118 with permission from The Royal Society of Chemistry.

exhibited different degrees of quenching behaviours, especially for NFZ and NFT. The relative emission intensity of I_{441}/I_{583} was utilized as the detectable signal to evaluate the sensing ability. As seen in Fig. 16c–e, all emission peaks obviously decreased with the continuously increasing amounts of CPFX and NFX, along with the obvious colour change from light yellow to pure white at the concentration of 4 mM, and then to indigo blue at 7 mM. The K_{sv} values and LOD values were 5.98 × 10^4 M^{-1} and 99 ppb toward NFZ, and 6.69 × 10^4 M^{-1} and 107 ppb toward NFZ, respectively, by analysing the peak at 545 nm. Additionally, the values of I_{441}/I_{583} had a fine linear relationship with the CPFX and NFX concentrations. The calculated K_{sv} and LOD values were 1.67 × 10^4 M^{-1} and 716 ppb toward CPFX, and 5.71 × 10^4 M^{-1} and 201 ppb toward NFX, respectively. The absorbing NFX and CPFX could emit blue luminescence, but no visible emission was found in NZF and NFT. Hence, only colour change of this composite was found in the NFX and CPFX aqueous solutions. This work demonstrates that dye@LMOFs are feasible indicators for monitoring antibiotics in water through their luminescence quenching behaviour and various colour changes by naked eyes.

Zhu *et al.* synthesized a novel dual-emissive ratio luminescent probe based on RhB-CDs@MOF (CDs = carbon dots) for antibiotic detection.[118] Unlike other dye@MOFs, this sensing composite can be prepared by post-synthetic modification. As

illustrated in Fig. 17a, a 3D porous Cu-MOF, Cu₂L(OH⁻) (**1**) (H₃L = 1,3-bis(40-carboxylic acid benzyloxy)-benzoic acid), was successfully prepared. It was then linked with RhB-CDs using [3-(2-aminoethylamino)propyl]tri-methoxysilane (AEATMS) as a binding agent to obtain the RhB-CDs@**1** composite. This composite indicated two broad luminescent bands at around 430 and 580 nm under the excitation at 355 nm with a pink colour. The luminescence emission remained the same as the original emission even after one week, illustrating the excellent luminescence stability. The emission peak at 580 nm presented an obvious decline toward NFZ, NFT, and TC. The K_{sv} values of NFT, NFZ, and TC were 2.09 × 10^4, 1.98 × 10^4, and 0.40 × 10^4 M^{-1}, with the LOD values of 0.31 mM (74 ppb), 0.33 mM (65 ppb), and 1.62 mM (777 ppb), respectively. Furthermore, this composite showed a "turn-on" behaviour at 430 nm and a clear "turn-off" luminescence at 580 nm in the CPFX and NFX aqueous solutions (Fig. 17b), leading to this composite being a potential ratiometric luminescence probe based on dual emission toward CPFX and NFX. There is a good linear relationship between the value of I_{430}/I_{580} and the concentration of CPFX and NFX under 90 mM (Fig. 17c), with the LOD values of 0.08 mM (25 ppb) for CPFX and 0.14 mM (44 ppb) for NFX. The K_{sv} values of CPFX and NFX were 2.5 × 10^4 and 1.38 × 10^4 M^{-1}, respectively. More interestingly, the CIE diagram and photographs under UV light showed that the colour of RhB-CDs@**1** changes from light pink to blue with the addition of NFX in Fig. 17d and e. Meanwhile, this probe exhibits the outstanding selectivity and stability even in domestic water. These results demonstrate that the synthesized RhB-CDs@**1** is

This journal is © the Partner Organisations 2020

Inorg. Chem. Front., 2020, **7**, 4293–4319 | **4309**

a luminescence probe toward nitrofurans and quinolones in water.

The above research studies demonstrated that the adsorbed or linked organic dyes in MOFs are an effective approach to construct LMOFs as luminescence probes in the detection of various antibiotics. Such functional LMOFs have potential applications in environmental protection and pollutant monitoring. In terms of the detection effectiveness, the luminescence performance of the luminescence composites can be designed and obtained by tuning various dyes, metal nodes, and organic ligands.

5. Metal–organic gel-based luminescence sensor

The International Union of Pure and Applied Chemistry (IUPAC) describes the gel as a 'non-fluid colloid network or polymer network that is expanded throughout its whole volume by a fluid'.[119] Recently, metal–organic gels (MOGs) have been considered a novel class of 3D soft supramolecular materials based on the coordination interaction of metal cations and organic ligands, which are analogous to the compositions and structures of MOFs. The comparison with the crystalline MOFs reveals that MOGs has larger porous structures, lower density, and easier formability, which contributes to their potential applications.[120] Nevertheless, MOGs are difficult to obtain and it is challenging to determine their exact structures to limit their widespread investigations. Therefore, the design and preparation of MOGs featuring the aimed functional property is still tricky and meaningful.

In 2017, Qin *et al.* synthesized a MOG(Al) gel by heating Al$(NO_3)_3$·$9H_2O$ and 1,3,5-benzentricarboxylic acid in ethanol, which can be used as a host material to prepare MOG(Eu) through the metal cation exchange process.[121] The PXRD data showed that MOG(Al) and MOG(Eu) xerogels were of low crystallinity with similar networks. The solid-state luminescence spectrum of MOG(Eu) had obvious emission peaks at 580, 590, 614, 653, and 701 nm from the Eu(III) cations with the quantum yield of 6.6% and long lifetime of 32.6 ns at room temperature by the reason of the highly effective energy transfer from the organic ligand to the Eu^{3+} cation. MOG(Eu) has the excellent luminescence detection ability toward a variety of antibiotics. The Stern–Volmer plots show the fine linear relationship in the low concentration range, but it clearly breaks away from the linear relation at high concentrations due to the dynamic guest molecular adsorption process. The MOG(Eu) xerogel possessed K_{sv} values of 2.9×10^4, 2.1×10^4, 2.3×10^4, and 1.4×10^4 M^{-1} towards RDZ, ODZ, MDZ and DTZ, respectively. In addition, the LOD values were estimated as 1.205 ppm for RDZ, 0.542 ppm for ODZ, 0.999 ppm for MDZ, and 0.377 ppm for DTZ. This work demonstrates that MOGs have excellent potential luminescence sensors for antibiotic detection.
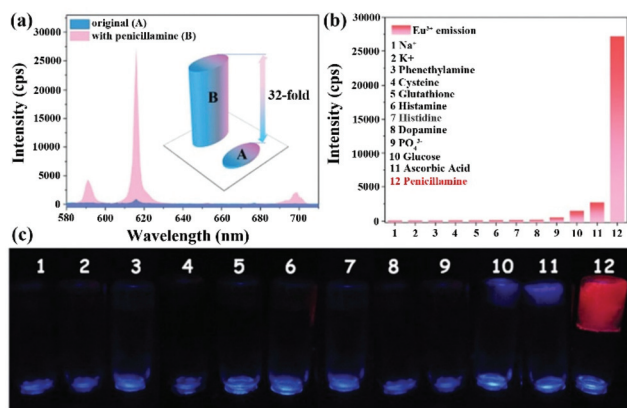
Another similar work was further reported by Qin and co-authors.[122] The targeted MOG(Tb) was generated by immer-

Fig. 18 (a) Synthetic illustration of gels with the photographs under day light and UV light. (b) Emission peaks of MOG(Tb) xerogel in multiple antibiotics aqueous solutions. (c) Concentration-dependent luminescence emission of MOG(Tb) xerogel in the SDZ aqueous solution. Reproduced from ref. 122 with permission from The Royal Society of Chemistry.

sing the MOG(Al) gel into the Tb$(NO_3)_3$ ethanol solution for one week through the metal node metathesis (Fig. 18a). The MOG(Tb) xerogel exhibited strong luminescence emissions at 615, 585, 544, and 491 nm from the f–f transitions of Tb^{3+}, which was enhanced by the "antenna effect" of the ligand. Additionally, the MOG(Tb) xerogel had a high quantum yield of 18.5% and long decay lifetime of 1.27 ns at room temperature by the reason of the efficient energy transfer from the sensitizer ligand to Tb^{3+} centre. The PXRD patterns and surface areas still showed no change in an aqueous solution with a wide pH range from 2 to 12 for 1 day at room temperature. The strong green luminescence and preferable stability offered the potential sensing ability toward antibiotics in water. As shown in Fig. 18b, the MOG(Tb) xerogel has the most sensitive luminescence behaviour to SDZ compared with other antibiotics. To further understand the sensing effect, the luminescence emissions were collected in SDZ with a concentration range of 0–0.4 mM (Fig. 18c). Due to the existence of the self-absorption or energy-transfer, the Stern–Volmer plots displayed a non-linear relationship. However, a fine linear relationship could be found in the low SMZ and SDZ concentration ranges. Based on the linear relationship, the K_{sv} values of the MOG(Tb) xerogel toward SMZ and SDZ are as high as 8.0×10^4 and 4.1×10^4 M^{-1}, respectively. In addition, the LOD are 0.086 ppm for SMZ and 0.218 ppm for SDZ based on $3S_b/K_{sv}$. This MOG(Tb) is an excellent candidate as a luminescence indicator for SDZ in water.

A 3D Eu-based MOF $[Eu_2(BPDC)(BDC)_2(H_2O)_2]_n$ (namely **1**) and hydrogel **1**@SA were synthesized by Lian and co-authors.[123] The hydrogel sample was amorphous and of pori-

4310 | *Inorg. Chem. Front.*, 2020, **7**, 4293–4319

This journal is © the Partner Organisations 2020

Fig. 19 (a) The increasing luminescence emission of **1**@SA hydrogel with PCL. (b) The emission intensity at 613 nm of **1**@SA hydrogel toward different analytes. (c) The corresponding photographs under UV lamp. Reproduced from ref. 123 with permission from The Royal Society of Chemistry.

ferous construction, which had an obvious red luminescence emission located at 578, 590, 613, 651 and 700 nm of the Eu^{3+} cations. Similar to most LMOFs, the luminescence emission can expeditiously and completely disappear upon the addition of the Fe^{3+} cation. Taking into account the high affinity between penicillamine (PCL) and Fe^{3+}, it may cause the luminescence "turn on" behaviour to emit red light. As shown in Fig. 19a, this hydrogel indicator exhibits a 32-fold amplification of the luminescence emission intensity toward PCL. Meanwhile, only PCL was able to induce the red luminescence, which was hardly changed even in the presence of other interfering substances (Fig. 19b and c). The emission intensity gradually increased with increasing PCL concentration in the range of 10^{-7}–10^{-2} M in water with a LOD value of 7.65 mM. In particular, hydrogel **1**@SA can quantitatively determinate PCL in serum, which still had the signal response at 8.74 mM. In addition, the hydrogel displayed an obviously increasing red color at high concentration. Thus, this novel hydrogel **1**@SA can diagnose PCL in water environment and actual serum.

According to these reports, MOGs are excellent candidates as luminescence sensor materials to discern antibiotics in the water environment. Nevertheless, the design and preparation of novel MOGs as probes are still a great challenge. On the other hand, MOGs based on the previously reported MOFs may be prepared by tuning the synthetic condition. Additionally, some reported MOGs can be used as host materials to immobilize the functional luminescence species to monitor antibiotics, which can uncover and widen the application fields of MOGs.

6.   LMOF thin film-based luminescence sensor

LMOFs have been widely prepared and used as luminescence sensors for monitoring various pollutants. However, most of

them are massive solid materials with poor dispersion and tend to fall down into the suspension. The instability of the LMOFs suspension will result in a lot of uncertainty during the sensing process. Reducing the crystal size into the micro-nano-scale through grinding and the microwave method is the most commonly used approach to enhance the dispersion and the stability of the suspension. Notably, if the crystal size is made too small for high dispersion, it will raise another conundrum to effectively separate these powders from the detection system. Recently, LMOF thin-films were prepared as sensing devices to detect contaminants, which can effectively solve the above problems. LMOF thin-films have various advantages, including their controlled shape and size, flexibility, stability, and repeatability. Some relative LMOF thin films have been fabricated *via* various synthetic strategies.[124–129] A representative work has been reported by Zhang and co-authors.[124] The 2,2′-biquinoline-4,4′-dicarboxylate (H_2BCA) ligand was utilized to coordinate with the Eu^{3+} cation to generate Eu-BCA, $[Eu_2(BCA)_3(H_2O)(DMF)_3]\cdot 0.5DMF\cdot H_2O$, with strong red luminescence emission. The Eu-BCA thin-film cannot be fabricated by the direct approach, but it can be obtained through an efficient strategy. As shown in Fig. 20a, Co_3O_4 nanowire arrays as interlayers are first coated on a stainless-steel wire mesh (SSWM), which is an important step to prepare the Eu-BCA thin-film. Co_3O_4 covered on SSWM is employed as the crystal nucleus to grow Eu-BCA by immersion into the precursor solution of MOF, which is able to fix onto SSWM to obtain the Eu-BCA thin-film. This film showed four emission peaks at 591, 615, 650, and 697 nm from the Eu^{3+} centre in water. Meanwhile, this Eu-BCA thin-film demonstrated preferable rollability and flexibility to easily increase the plasticity. The fabricated film had excellent water stability, and demonstrated stable luminescence in water for one week. The peak located at 615 nm is the most prominent emission, and was utilized as the detectable signal. This luminescence
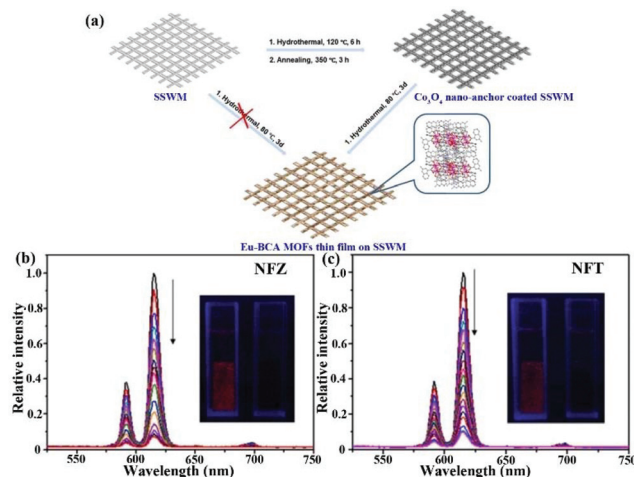
Fig. 20 (a) Preparation process of Eu-BCA thin film. (b and c) Luminescence emissions of this film in NFZ and NFT aqueous solutions. Reproduced from ref. 124 with permission from Wiley-VCH.

This journal is © the Partner Organisations 2020

Inorg. Chem. Front., 2020, **7**, 4293–4319 | **4311**

film displayed different quenching efficiencies in various antibiotics and aqueous solutions, especially for NFT and NFZ, because the electron-deficient nitro-group can accelerate the electron transfer from MOF to both antibiotics. As seen in Fig. 20b and c, the emission spectra gradually decreased with the incremental concentration of antibiotics from 0 to 600 mm. The K_{sv} values of NFZ and NFT were 2.2×10^4 and 1.6×10^4 M^{-1}, and the corresponding LOD values were 0.21 and 0.16 μM, respectively. In natural water, the K_{sv} values of NFZ and NFT were 1.9×10^4 and 1.7×10^4 M^{-1}, respectively. This Eu-BCA thin-film had good selectivity and reusability. More importantly, it showed excellent sensing ability toward NFZ in bovine serum. The Eu-BCA thin-film is an available diagnostic sensor device for NFA in water and food.

Gao *et al.* developed a simple and easy way to fabricate mixed-crystal Ln-MOFs thin films on the Indium–Tin Oxide (ITO) glass support as luminescence sensor devices (Fig. 21a).[125] The nanocrystal Ln-MOFs with hexagonal morphology and a size of 150 ± 50 nm retained the original structure after the fabrication process. The SEM image illustrates that the surface of the mixed-crystal Ln-MOF thin film was complete, continuous, and pyknotic (Fig. 21b). Tb-MOF displayed the four characteristic emissions of the Tb^{3+} cation at 489, 547, 587, and 622 nm, while Eu-MOF showed the characteristic line-like peaks located at 592, 619, 654, and 703 nm. A series of mixed-crystal Ln-MOFs were successfully obtained by adjusting the ratio of Eu^{3+} and Tb^{3+} cations, which all exhibited emission peaks from both Eu^{3+} and Tb^{3+} cations. $Eu_{0.1}Tb_{0.9}$-MOF was selected as the mixed Ln-MOF to fabricate the MOF thin-film. Meanwhile, visible emission peaks at 547 nm from the $^5D_4 \rightarrow {}^7F_5$ transition of the Tb^{3+} cation and 619 nm originating from the $^5D_0 \rightarrow {}^7F_2$ transition of the Eu^{3+} cation were utilized to analyse the sensing behaviour of this film toward various analytes. As shown in Fig. 21c, this film showed guest-dependent emission through the interaction between host and guest. More interestingly, the optical images

still exhibited obvious changes and entirely different colours, such as yellow, green, and red (Fig. 21d). Due to the merit of the film, this film device was easily and feasibly separated from the detectable system and had excellent recyclability. The above results clearly illustrate that this mixed-crystal Ln-MOF thin film is a luminescence indictor toward various analytes in water by luminescence quenching and obvious colour variance.

Li and co-authors synthesized a Tb-based MOF, Tb(HL)L (H₂O) (H₂L = salicylic acid), with emission peaks at 486, 542, 581 and 618 nm.[126] The luminescence property of the Tb-based LMOF was almost unaffected in most anions and cations, as well as antibiotics. However, an obvious luminescence quenching performance was detected in the OTC and TC aqueous solutions, illustrating the excellent stability and potential sensing ability toward OTC and TC. From the gradual addition of OTC and TC, the luminescence intensities of Tb-MOF exhibited an obvious luminescence-quenching phenomenon with the dribbling away of the green colour (Fig. 22a and c). The fine linear relationship between I_0/I of Tb-MOF and the increasing concentrations can be obtained and used to evaluate the sensing ability of Tb-MOF toward OTC and TC. The K_{sv} values of Tb-MOF were 2.18×10^4 M^{-1} for OTC and 1.39×10^4 M^{-1} for TC in deionized water (Fig. 22b and d). The corresponding LOD values were calculated to be 1.95 and 2.77 nM, respectively. Meanwhile, this luminescence sensor could
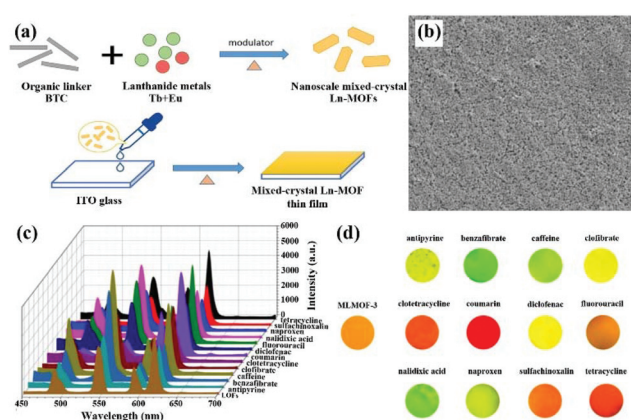

Fig. 21 (a) The synthetic process of the nanoscale mixed-crystal Ln-MOF thin film. (b) The SEM image of this film surface. (c) Emission spectra and (d) optical images of this Ln-MOF thin film in different aqueous solutions with different analytes. Reproduced from ref. 125 with permission from Elsevier.

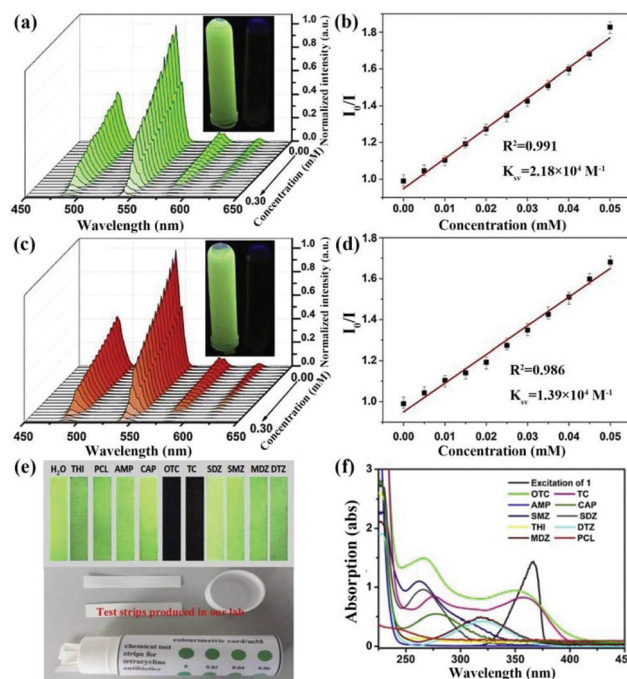**Fig. 22** Emission peaks and linear relationships between I_0/I of Tb-MOF and the increasing concentrations of (a and b) OTC and (c and d) TC with the luminescence pictures under UV lamp. (e) The corresponding optical pictures of the Tb-MOF-based test strips for monitoring multiple antibiotics. (f) UV-Vis spectra of selected antibiotics and the excitation band of Tb-MOF. Reproduced from ref. 126 with permission from Elsevier.

monitor OTC and TC in real Pearl River water. The used samples were easily collected by centrifugation to recover the luminescence emission after washing with fresh water under ultrasound. It showed excellent reusability for at least thirty cycles. The Tb-MOF-based test strips can be prepared by an easy immersion way, and were employed as a portable device to detect multifarious antibiotics at the low-concentration aqueous solution within only 1 min. The result illustrates that only OTC and TC enabled the quenching of the green luminescence of test strips under UV lamp by naked eyes (Fig. 22e), implying the promising practical application in the detection of OTC and TC. The quenching reason is primally due to the UV excitation energy competition between Tb-MOF and the aqueous solution of OTC and TC to reduce the "antenna effect" in MOF (Fig. 22f).

Additionally, mixed matrix membranes (MMMs) are a kind of common composite materials, which is able to homogeneously import filler particles into the polymeric matrix. Thus, these composites possessed both properties of polymer and filler. From 2017, three examples of Ln(III)-based luminescence MMMs have been designed and prepared as indicators toward antibiotics in water.[127–129] For example, Zhang and co-authors reported on a Tb-MOF $[Tb_2(AIP)_2(H_2O)_{10}]\cdot(AIP)\cdot4H_2O$ (Tb-AIP, AIP = 5-aminoisophthalate) with green luminescence, which was utilized as powder fillers to incorporate into the low-cost and clear polymer of poly(methyl methacrylate) (PMMA) chloroform solution.[127] The mixed slurry was further dropped onto the glass, and then dried in a 40 °C oven overnight (Fig. 23a). The optical images under natural light and UV lamp at 365 nm showed that the Tb-AIP-based MMMs with 9.1% MOF was the most suitable test device for the sensing experiments (Fig. 23b and c). This fabricated film in water showed the distinct green characteristic peaks from Tb-AIP at room temperature. The most prominent peak of 543 nm was con-

sidered as the analytic signal for the sensing process. As seen in Fig. 23d and e, this film exhibited the concentration-depend luminescence emission. The quenching behaviour can be found in NFZ or NFT aqueous solution with the K_{sv} and LOD values of 2.8×10^4 M^{-1} and 0.35 μM for NFZ, and 4.0×10^4 M^{-1} and 0.30 μM for NFT, respectively. Also, it demonstrated good reusability and selectivity toward NFZ and NFT. It is notable that this film can quantitatively and accurately detect NFT in the real bovine serum samples.

Meanwhile, another two similar reports still showed the sensing ability toward target antibiotics.[128,129] The result illustrates that Ln(III)-based MMMs have many advantages, such as high stability, outstanding reproducibility, easy operability, excellent selectivity and sensitivity. In addition, the fabricated film device feasibly separates from the detectable system and recovers the luminescent property. Therefore, luminescence films based on Ln-MOFs are portable and available devices, which have potential applications in the luminescence detection of antibiotics in water systems for the analysis of food and water environment.

7. Conclusions and perspectives

Herein, we summarize various classes of LMOFs for monitoring antibiotics, including: (1) LMOFs based on luminescent organic ligands; (2) LMOFs based on luminescent metal nodes; (3) Ln(III)-doped or adsorbed/linked lumophores based LMOFs; (4) MOGs-based luminescence sensor, and (5) LMOF films. LMOFs have many advantages for monitoring antibiotics, such as their strong luminescence intensity, outstanding sensitive and selectivity, exquisite designability, and multiformity. The multi-emissive LMOFs have the excellent specificity to recognise target antibiotics. In particular, MOGs and LMOFs-based thin films can enhance the sensing ability, portability and operability. Porous structures further facilitate the diversity and controllability of luminescence performance through the host–guest interaction. LMOFs will take a solid step forward in the water and environmental protection. Moreover, their devices have broad and huge potential use value.

In spite of the abovementioned virtues, several limitations in LMOFs obviously restrict their applications, e.g., poor water stability and dispersancy. Some LMOFs can be fabricated into thin-films or with reduced crystal size to solve these problems, but more efficient and universal methods are needed to investigate a solution to these problems. In addition, most attention has been focused on the preparation of novel MOFs with the shallow detection research of antibiotics. The real detection mechanism of LMOFs toward different antibiotic needs more in-depth research, reliable experimental and theoretical analysis. Meanwhile, the structure–function relationship is still under exploration and development for monitoring antibiotics, which can guide the synthesis of more efficient LMOFs to detect antibiotics. Hence, more research studies should be done to utilize LMOFs and their devices for monitoring anti-

Fig. 23 (a) The preparation process of Tb-AIP MMMs. Images of Tb-AIP MMMs by varying the additional amounts of MOF powders (b) under natural light and (c) UV lamp at 365 nm. Emission spectra of Tb-AIP MMMs upon increasing concentrations of (d) NFZ and (e) NFT. Reproduced from ref. 127 with permission from Elsevier.

This journal is © the Partner Organisations 2020

Inorg. Chem. Front., 2020, **7**, 4293–4319 | **4313**

biotics in the water environment and food safety analysis, which is of significant meaning in both academic and practical fields. We think LMOFs will have a bright future in the sensing application of antibiotics.

Conflicts of interest

There are no conflicts to declare.

Acknowledgements

Notes and references

1 T. J. Everage, R. Boopathy, R. Nathaniel, G. LaFleur and J. Doucet, A survey of antibiotic-resistant bacteria in a sewage treatment plant in Thibodaux, Louisiana, USA, *Int. Biodeterior. Biodegrad.*, 2014, **95**, 2–10.

2 J. Carcía, M. J. García-Galán, J. W. Day, R. Boopathy, J. R. White, S. Wallace and R. G. Hunter, A review of emerging organic contaminants (EOCs), antibiotic resistant bacteria (ARB), and antibiotic resistance genes (ARGs) in the environment: Increasing removal with wetlands and reducing environmental impacts, *Bioresour. Technol.*, 2020, **307**, 123228.

3 F. O. Gudda, M. G. Waigi, W. S. Odinga, B. Yang, L. Carter and Y. Gao, Antibiotic-contaminated wastewater irrigated vegetables pose resistance selection risks to the gut microbiome, *Environ. Pollut.*, 2020, **264**, 114752.

4 Y. Hsia, M. Sharland, C. Jackson, L. C. K. Wong, N. Magrini and J. A. Bielicki, Consumption of oral antibiotic formulations for young children according to the WHO Access, Watch, Reserve (AWaRe) antibiotic groups: an analysis of sales data from 70 middle-income and high-income countries, *Lancet Infect. Dis.*, 2019, **19**, 67–75.

5 N. Le-Minh, S. J. Khan, J. E. Drewes and R. M. Stuetz, Fate of antibiotics during municipal water recycling treatment processes, *Water Res.*, 2010, **44**, 4295–4323.

6 A. S. Oberoi, Y. Jia, H. Zhang, S. K. Khanal and H. Lu, Insights into the fate and removal of antibiotics in engineered biological treatment systems: A critical review, *Environ. Sci. Technol.*, 2019, **53**, 7234–7264.

7 S. D. Shifflett and J. Schubauer-Berigan, Assessing the risk of utilizing tidal coastal wetlands for wastewater management, *J. Environ. Manage.*, 2019, **236**, 269–279.

8 Y. Shen, R. Zhuan, L. Chu, X. Xiang, H. Sun and J. Wang, Inactivation of antibiotic resistance genes in antibiotic fermentation residues by ionizing radiation: Exploring the development of recycling economy in antibiotic pharmaceutical factory, *Waste Manage.*, 2019, **84**, 141–146.

9 CDC, *Antibiotic Resistance Threats in the United States, 2019*, U.S. Department of Health and Human Services, CDC, Atlanta, GA, 2019, p. 148.

10 Y. Ben, C. Fu, M. Hu, L. Liu, M. H. Wong and C. Zheng, Human health risk assessment of antibiotic resistance associated with antibiotic residues in the environment: A review, *Environ. Res.*, 2019, **169**, 483–493.

11 L. Tian, S. Bayen and V. Yaylayan, Thermal degradation of five veterinary and human pharmaceuticals using pyrolysis-GC/MS, *J. Anal. Appl. Pyrolysis*, 2017, **127**, 120–125.

12 W. M. A. Niessen, Analysis of antibiotics by liquid chromatography mass spectrometry, *J. Chromatogr. A*, 1998, **812**, 53–75.

13 M. L. Castillo-Garcia, M. P. Aguilar-Caballos and A. Gomez-Hens, Determination of veterinary penicillin antibiotics by fast high-resolution liquid chromatography and luminescence detection, *Talanta*, 2017, **170**, 343–349.

14 N. Sharma, S. P. Selvam and K. Yun, Electrochemical detection of amikacin sulphate using reduced graphene oxide and silver nanoparticles nanocomposite, *Appl. Surf. Sci.*, 2020, **512**, 145742.

15 Y.-Q. Hong, X. Guo, G.-H. Chen, J.-W. Zhou, X.-M. Zou, X. Liao and T. Hou, Determination of five macrolide antibiotic residues in milk by micellar electrokinetic capillary chromatography with field amplified sample stacking, *J. Food Saf.*, 2018, **38**, e12382.

16 J. Xu, B. Zhang, L. Jia, N. Bi and T. Zhao, Metal-enhanced fluorescence detection and degradation of tetracycline by silver nanoparticle-encapsulated halloysite nano-lumen, *J. Hazard. Mater.*, 2020, **386**, 121630.

17 G. Kaur, M. Chaudhary, K. C. Jena and N. Singh, Terbium (III)-coated carbon quantum dots for the detection of clomipramine through aggregation-induced emission from the analyte, *New J. Chem.*, 2020, **44**, 10536–10544.

18 J. Zdunek, E. Benito-Pena, A. Linares, A. Falcimaigne-Cordin, G. Orellana, K. Haupt and M. C. Moreno-Bondi, Surface-imprinted nanofilaments for europium-amplified luminescent detection of fluoroquinolone antibiotics, *Chem. – Eur. J.*, 2013, **19**, 10209–10216.

19 C. Vakh, A. Pochivalov, S. Koronkiewicz, S. Kalinowski, V. Postnov and A. Bulatov, A chemiluminescence method for screening of fluoroquinolones in milk samples based on a multi-pumping flow system, *Food Chem.*, 2019, **270**, 10–16.

20 Y. Sun, Y. Dai, X. Zhu, R. Han, X. Wang and C. Luo, A nanocomposite prepared from bifunctionalized ionic liquid, chitosan, graphene oxide and magnetic nanoparticles for aptamer-based assay of tetracycline by chemiluminescence, *Microchim. Acta*, 2020, **187**, 63.

21 M. Amjadi, T. Hallaj and F. Mirbirang, A chemiluminescence reaction consisting of manganese(IV), sodium sulfite, and sulfur- and nitrogen-doped carbon quantum dots, and its application for the determination of oxytetracycline, *Microchim. Acta*, 2020, **187**, 191.

22 A.-M. Maciuca, A.-C. Munteanu and V. Uivarosi, Quinolone complexes with lanthanide ions: An insight

into their analytical applications and biological activity, *Molecules*, 2020, **25**, 1347.

23 F. Tewes, T. F. Bahamondez-Canas, D. Moraga-Espinoza, H. D. C. Smyth and A. B. Watts, In vivo efficacy of a dry powder formulation of ciprofloxacin-copper complex in a chronic lung infection model of bioluminescent Pseudomonas aeruginosa, *Eur. J. Pharm. Biopharm.*, 2020, **152**, 210–217.

24 S. Chand, A. Pal, R. Saha, P. Das, R. Sahoo, P. K. Chattaraj and M. C. Das, Two closely related Zn(II)-MOFs for their large difference in CO_2 uptake capacities and selective CO_2 sorption, *Inorg. Chem.*, 2020, **59**, 7056–7066.

25 W. Fan, S. Yuan, W. Wang, L. Feng, X. Liu, X. Zhang, X. Wang, Z. Kang, F. Dai, D. Yuan, D. Sun and H.-C. Zhou, Optimizing multivariate metal-organic frameworks for efficient C_2H_2/CO_2 separation, *J. Am. Chem. Soc.*, 2020, **142**, 8728–8737.

26 S. Rauf, M. T. Vijjapu, M. A. Andres, I. Gascon, O. Roubeau, M. Eddaoudi and K. N. Salama, Highly selective metal-organic framework textile humidity sensor, *ACS Appl. Mater. Interfaces*, 2020, **12**, 29999–30006.

27 R. Dalapati, S. Nandi, K. V. Hecke and S. Biswas, Fluorescence modulation of an aggregation-induced emission active ligand via rigidification in a coordination polymer and its application in singlet oxygen sensing, *Cryst. Growth Des.*, 2019, **19**, 6388–6397.

28 H. He, Q. Sun, W. Gao, J. A. Perman, F. Sun, G. Zhu, B. Aguila, K. Forrest, B. Space and S. Ma, A stable metal-organic framework featuring a local buffer rnvironment for carbon dioxide fixation, *Angew. Chem., Int. Ed.*, 2018, **57**, 4657–4662.

29 H. He, J. A. Perman, G. Zhu and S. Ma, Metal-organic frameworks for CO_2 chemical transformations, *Small*, 2016, **12**, 6309–6324.

30 Y. Wang, N. Zhang, E. Zhang, Y. Han, Z. Qi, M. B. Ansorge-Schumacher, Y. Ge and C. Wu, Heterogeneous metal-organic-framework-based biohybrid catalysts for cascade reactions in organic solvent, *Chem. – Eur. J.*, 2019, **25**, 1716–1721.

31 M. Naseri, F. Pitzalis, C. Carucci, L. Medda, L. Fotouhi, E. Magner and A. Salis, Lipase and laccase encapsulated on zeolite imidazolate framework: Enzyme activity and stability from voltammetric measurements, *ChemCatChem*, 2018, **10**, 5425–5433.

32 C.-H. Liu, Q.-L. Guan, X.-D. Yang, F.-Y. Bai, L.-X. Sun and Y.-H. Xing, Polyiodine-modified 1,3,5-benzenetricarboxylic acid framework Zn(II)/Cd(II) complexes as highly selective fluorescence sensors for thiamine hydrochloride, NACs, and Fe^{3+}/Zn^{2+}, *Inorg. Chem.*, 2020, **59**, 8081–8098.

33 H. He, Y. Song, F. Sun, N. Zhao and G. Zhu, Sorption properties and nitroaromatic explosives sensing based on two isostructural metal-organic frameworks, *Cryst. Growth Des.*, 2015, **15**, 2033–2038.

34 Y. Yu, Y. Wang, H. Yan, J. Lu, H. Liu, Y. Li, S. Wang, D. Li, J. Dou, L. Yang and Z. Zhou, Multiresponsive luminescent sensitivities of a 3D Cd-CP with visual turn-on and ratio-

metric sensing toward Al^{3+} and Cr^{3+} as well as turn-off sensing toward Fe^{3+}, *Inorg. Chem.*, 2020, **59**, 3828–3837.

35 R. Dalapati, S. Nandi and S. Biswas, Post-synthetic modification of a metal-organic framework with a chemodosimeter for the rapid detection of lethal cyanideviadual emission, *Dalton Trans.*, 2020, **49**, 8684–8692.

36 L. Yu, H. Wang, W. Liu, S. J. Teat and J. Li, Blue-light-excitable, quantum yield enhanced, yellow-emitting, zirconium-based metal-organic framework phosphors formed by immobilizing organic chromophores, *Cryst. Growth Des.*, 2019, **19**, 6850–6854.

37 J. Heine and K. Muller-Buschbaum, Engineering metal-based luminescence in coordination polymers and metal-organic frameworks, *Chem. Soc. Rev.*, 2013, **42**, 9232–9242.

38 H. He, F. Sun, T. Borhigin, N. Zhao and G. Zhu, Tunable colors and white-light emission based on a microporous luminescent Zn(II)-MOF, *Dalton Trans.*, 2014, **43**, 3716–3721.

39 L. Xu, M. Pan, G. Fang and S. Wang, Carbon dots embedded metal-organic framework@molecularly imprinted nanoparticles for highly sensitive and selective detection of quercetin, *Sens. Actuators, B*, 2019, **286**, 321–327.

40 L. Guo, Y. Liu, R. Kong, G. Chen, H. Wang, X. Wang, L. Xia and F. Qu, Turn-on fluorescence detection of beta-glucuronidase using RhB@MOF-5 as an ultrasensitive nanoprobe, *Sens. Actuators, B*, 2019, **295**, 1–6.

41 P. Mahata, S. K. Mondal, D. K. Singha and P. Majee, Luminescent rare-earth-based MOFs as optical sensors, *Dalton Trans.*, 2017, **46**, 301–328.

42 H.-Q. Yin and X.-B. Yin, Metal-organic frameworks with multiple luminescence emissions: Designs and applications, *Acc. Chem. Res.*, 2020, **53**, 485–495.

43 P. Samanta, S. Let, W. Mandal, S. Dutta and S. K. Ghosh, Luminescent metal-organic frameworks (LMOFs) as potential probes for the recognition of cationic water pollutants, *Inorg. Chem. Front.*, 2020, **7**, 1801–1821.

44 B. Wang, X.-L. Lv, D. Feng, L.-H. Xie, J. Zhang, M. Li, Y. Xie, J.-R. Li and H.-C. Zhou, Highly stable Zr(IV)-based metal-organic frameworks for the detection and removal of antibiotics and organic explosives in water, *J. Am. Chem. Soc.*, 2016, **138**, 6204–6216.

45 F.-M. Wang, L. Zhou, W. P. Lustig, Z. Hu, J.-F. Li, B.-X. Hu, L.-Z. Chen and J. Li, Highly luminescent metal-organic frameworks based on an aggregation-induced emission ligand as chemical sensors for nitroaromatic compounds, *Cryst. Growth Des.*, 2018, **18**, 5166–5173.

46 J. Li, S. Yuan, J.-S. Qin, L. Huang, R. Bose, J. Pang, P. Zhang, Z. Xiao, K. Tan, A. V. Malko, T. Cagin and H.-C. Zhou, Fluorescence enhancement in the solid State by isolating perylene fluorophores in metal-organic frameworks, *ACS Appl. Mater. Interfaces*, 2020, **12**, 26727–26732.

47 B. B. Rath and J. J. Vittal, Water stable Zn(II) metal-organic framework as a selective and sensitive luminescent probe for Fe(III) and chromate ions, *Inorg. Chem.*, 2020, **59**, 8818–8826.

This journal is © the Partner Organisations 2020

Inorg. Chem. Front., 2020, **7**, 4293–4319 | **4315**

48 S. A. A. Razavi and A. Morsali, Metal ion detection using luminescent-MOFs: Principles, strategies and roadmap, *Coord. Chem. Rev.*, 2020, **415**, 213299.

49 S.-L. Hou, J. Dong, X.-L. Jiang, Z.-H. Jiao, C.-M. Wang and B. Zhao, Interpenetration-dependent luminescent probe in indium-organic frameworks for selectively detecting nitrofurazone in water, *Anal. Chem.*, 2018, **90**, 1516–1519.

50 Z. Zhou, M.-L. Han, H.-R. Fu, L.-F. Ma, F. Luo and D.-S. Li, Engineering design toward exploring the functional group substitution in 1D channels of Zn-organic frameworks upon nitro explosives and antibiotics detection, *Dalton Trans.*, 2018, **47**, 5359–5365.

51 H. He, Q.-Q. Zhu, M.-T. Guo, Q.-S. Zhou, J. Chen, C.-P. Li and M. Du, Doubly interpenetrated Zn_4O-based metal-organic framework for CO_2 chemical transformation and antibiotic sensing, *Cryst. Growth Des.*, 2019, **19**, 5228–5236.

52 H. He, Y.-Q. Xue, S.-Q. Wang, Q.-Q. Zhu, J. Chen, C.-P. Li and M. Du, A double-walled bimetal-organic framework for antibiotics sensing and size-selective catalysis, *Inorg. Chem.*, 2018, **57**, 15062–15068.

53 H. He, Q.-Q. Zhu, F. Sun and G. Zhu, Two 3D metal-organic frameworks based on Co(II) and Zn(II) clusters for Knoevenagel condensation reaction and highly selective luminescence sensing, *Cryst. Growth Des.*, 2018, **18**, 5573–5581.

54 Q.-Q. Zhu, Q.-S. Zhou, H.-W. Zhang, W.-W. Zhang, D.-Q. Lu, M.-T. Guo, Y. Yuan, F. Sun and H. He, Design and construction of a metal-organic framework as an efficient luminescent sensor for detecting antibiotics, *Inorg. Chem.*, 2020, **59**, 1323–1331.

55 D. Zhao, X.-H. Liu, Y. Zhao, P. Wang, Y. Liu, M. Azam, S. I. Al-Resayes, Y. Lu and W.-Y. Sun, Luminescent Cd(II)-organic frameworks with chelating NH_2 sites for selective detection of Fe(III) and antibiotics, *J. Mater. Chem. A*, 2017, **5**, 15797–15807.

56 L.-Q. Zhang, X.-W. Wang, L. Gu, Y.-H. Yu and J.-S. Gao, Three pairs of luminescent coordination polymers based on Co^{II} and Cd^{II} clusters for the detection of antibiotics, pesticides and chiral nitro aromatic compounds, *RSC Adv.*, 2020, **10**, 9476–9485.

57 J. Li, T.-J. Chen, S. Han and L.-F. Song, Four Zn(II)-organic frameworks as luminescent probe for highly selectivity detection of Cr-VI ions and antibiotics, *J. Solid State Chem.*, 2019, **277**, 107–114.

58 J.-L. Gu, X.-W. Tao, Q.-Q. Tu, A.-L. Cheng and E.-Q. Gao, Two sulfone-functionalized Zn(II)-coordination polymers as luminescent sensors for sensitive and rapid detection of nitrofurans antibiotics, *J. Solid State Chem.*, 2020, **286**, 121318.

59 Y.-L. Xu, Y. Liu, X.-H. Liu, Y. Zhao, P. Wang, Z.-L. Wang and W.-Y. Sun, Novel cadmium(II) frameworks with mixed carboxylate and imidazole-containing ligands for selective detection of antibiotics, *Polyhedron*, 2018, **154**, 350–356.

60 X.-Q. Yao, G.-B. Xiao, H. Xie, D.-D. Qin, H.-C. Ma, J.-C. Liu and P.-J. Yan, Two triphenylamine-based luminescent metal–organic frameworks as a dual-functional sensor for the detection of nitroaromatic compounds and ofloxacin antibiotic, *CrystEngComm*, 2019, **21**, 2559–2570.

61 J. Wang, N.-N. Chen, C.-D. Pan, C. Zhang and L. Fan, Selective fluorescence sensing properties of a novel two-fold interpenetrating coordination polymer, *New J. Chem.*, 2020, **44**, 9411–9418.

62 H. He, Q.-Q. Zhu, C.-P. Li and M. Du, Design of a highly-stable pillar-layer zinc(II) porous framework for rapid, reversible, and multi-responsive luminescent sensor in water, *Cryst. Growth Des.*, 2019, **19**, 694–703.

63 B.-X. Dong, Y.-M. Pan, W.-L. Liu and Y.-L. Teng, An ultra-stable luminescent metal-organic framework for selective sensing of nitroaromatic compounds and nitroimidazole-based drug molecules, *Cryst. Growth Des.*, 2018, **18**, 431–440.

64 J. Sun, P. Guo, M. Liu and H. Li, A novel cucurbit[6]uril-based supramolecular coordination assembly as a multi-responsive luminescent sensor for Fe^{3+}, $Cr_2O_7^{2-}$ and iso-quinoline antibiotics in aqueous medium, *J. Mater. Chem. C*, 2019, **7**, 8992–8999.

65 L. Shi, M. Liu and H. Li, A cucurbit[6]uril-based supramolecular assembly as a highly sensitive and quickly responsive luminescent sensor for the detection of fluoroquinolone antibiotics in simulated wastewater, *CrystEngComm*, 2020, **22**, 3753–3758.

66 W.-B. Zhong, R.-X. Li, J. Lv, T. He, M.-M. Xu, B. Wang, L.-H. Xie and J.-R. Li, Two isomeric In(III)-MOFs: unexpected stability difference and selective fluorescence detection of fluoroquinolone antibiotics in water, *Inorg. Chem. Front.*, 2020, **7**, 1161–1171.

67 F. Guo, C. Su, Y. Fan, W. Shi and X. Zhang, Construction of a dual-response luminescent metal-organic framework with excellent stability for detecting Fe^{3+} and antibiotic with high selectivity and sensitivity, *J. Solid State Chem.*, 2020, **284**, 121183.

68 J. Wang, Q. Zha, G. Qin and Y. Ni, A novel Zn(II)-based metal-organic framework as a high selective and sensitive sensor for fluorescent detections of aromatic nitrophenols and antibiotic metronidazole, *Talanta*, 2020, **211**, 120742.

69 P. Li, M.-Y. Guo, L.-L. Gao, X.-M. Yin, S.-L. Yang, R. Bu and E.-Q. Gao, Photoresponsivity and antibiotic sensing properties of an entangled tris(pyridinium)-based metal–organic framework, *Dalton Trans.*, 2020, **49**, 7488–7495.

70 P. Guo, M. Liu and L. Shi, A Zn-based coordination polymer as a luminescent sensor for simple and sensitive detecting of sulfonamides antibiotics and nitroaromatic, *J. Solid State Chem.*, 2020, **286**, 121247.

71 B. Zhang, P.-Y. Guo, L.-N. Ma, B. Liu, L. Hou and T.-Y. Wang, Two robust In(III)-based metal-organic frameworks with higher gas separation, efficient carbon dioxide conversion, and rapid detection of antibiotics, *Inorg. Chem.*, 2020, **59**, 5231–5239.

72 N. Xu, Q. Zhang, B. Hou, Q. Cheng and G. Zhang, A novel magnesium metal-organic framework as a multiresponsive luminescent sensor for Fe(III) ions, pesticides, and

4316 | *Inorg. Chem. Front.*, 2020, **7**, 4293–4319

This journal is © the Partner Organisations 2020

antibiotics with high selectivity and sensitivity, *Inorg. Chem.*, 2018, **57**, 13330–13340.

73 Z.-W. Zhai, S.-H. Yang, M. Cao, L.-K. Li, C.-X. Du and S.-Q. Zang, Rational design of three two-fold interpenetrated metal-organic frameworks: Luminescent Zn/Cd-metal-organic frameworks for detection of 2,4,6-trinitrophenol and nitrofurazone in the aqueous phase, *Cryst. Growth Des.*, 2018, **18**, 7173–7182.

74 X.-D. Zhu, K. Zhang, Y. Wang, W.-W. Long, R.-J. Sa, T.-F. Liu and J. Lü, Fluorescent metal-organic framework (MOF) as a highly sensitive and quickly responsive chemical sensor for the detection of antibiotics in simulated wastewater, *Inorg. Chem.*, 2018, **57**, 1060–1065.

75 F. Guo, C. Su, Y. Fan, W. Shi and X. Zhang, Rational design and synthesis of a stable pillar-layer Na(I)-organic framework as a multi-responsive luminescent sensor in aqueous solutions, *Spectrochim. Acta, Part A*, 2020, **230**, 118106.

76 Y. Chen, J. W. Y. Lam, R. T. K. Kwok and B. Z. Tang, Aggregation-induced emission: fundamental understanding and future developments, *Mater. Horiz.*, 2019, **6**, 428–433.

77 Y. Bai, Y. Dou, L.-H. Xie, W. Rutledge, J.-R. Li and H.-C. Zhou, Zr-based metal–organic frameworks: design, synthesis, structure, and applications, *Chem. Soc. Rev.*, 2016, **45**, 2327–2367.

78 X.-G. Liu, C.-L. Tao, H.-Q. Yu, B. Chen, Z. Liu, G.-P. Zhu, Z. Zhao, L. Shen and B. Z. Tang, A new luminescent metal–organic framework based on dicarboxyl-substituted tetraphenylethene for efficient detection of nitro-containing explosives and antibiotics in aqueous media, *J. Mater. Chem. C*, 2018, **6**, 2983–2988.

79 Y. Zhou, Q. Yang, D. Zhang, N. Gan, Q. Li and J. Cuan, Detection and removal of antibiotic tetracycline in water with a highly stable luminescent MOF, *Sens. Actuators, B*, 2018, **262**, 137–143.

80 Y. Zhao, Y.-J. Wang, N. Wang, P. Zheng, H.-R. Fu, M.-L. Han, L.-F. Ma and L.-Y. Wang, Tetraphenylethylene-decorated metal-organic frameworks as energy-transfer platform for the detection of nitro-antibiotics and white-light emission, *Inorg. Chem.*, 2019, **58**, 12700–12706.

81 E. Lee, H. Ju, J. H. Jung, M. Ikeda, Y. Habata and S. S. Lee, Conventional and mechanochemical syntheses of copper (I) iodide luminescent MOF with bis(amidoquinoline) and its application for the detection of amino acid in aqueous solution, *Inorg. Chem.*, 2019, **58**, 1177–1183.

82 B.-C. Tzeng and J.-F. Lin, Crystal-engineering and luminescence studies of 1,3,5-tris(3-pyridylethynyl)benzene or 1,3,5-tris(4-pyridylethynyl)benzene with copper(I) iodides, *Dalton Trans.*, 2019, **48**, 4046–4057.

83 Z. Fu, J. Lin, L. Wang, C. Li, W. Yan and T. Wu, Cuprous iodide pseudopolymorphs based on imidazole ligand and their luminescence thermochromism, *Cryst. Growth Des.*, 2016, **16**, 2322–2327.

84 G.-N. Liu, R.-Y. Zhao, R.-D. Xu, X. Zhang, X.-N. Tang, Q.-J. Dan, Y.-W. Wei, Y.-Y. Tu, Q.-B. Bo and C. Li, A novel tetranuclear copper(I) iodide metal-organic cluster [Cu₄I₄(Ligand)₅] with highly selective luminescence detection of antibiotic, *Cryst. Growth Des.*, 2018, **18**, 5441–5448.

85 G.-N. Liu, R.-D. Xu, R.-Y. Zhao, Y. Sun, Q.-B. Bo, Z.-Y. Duan, Y.-H. Li, Y.-Y. Wang, Q. Wu and C. Li, Hybrid copper iodide cluster-based pellet sensor for highly selective optical detection of o-nitrophenol and tetracycline hydrochloride in aqueous solution, *ACS Sustainable Chem. Eng.*, 2019, **7**, 18863–18873.

86 A. Lapprand, M. Dutartre, N. Khiri, E. Levert, D. Fortin, Y. Rousselin, A. Soldera, S. Juge and P. D. Harvey, Luminescent P-chirogenic copper clusters, *Inorg. Chem.*, 2013, **52**, 7958–7967.

87 W. Liu, Y. Fang, G. Z. Wei, S. J. Teat, K. C. Xiong, Z. C. Hu, W. P. Lustig and J. Li, A family of highly efficient CuI-based lighting phosphors prepared by a systematic, bottom-up synthetic approach, *J. Am. Chem. Soc.*, 2015, **137**, 9400–9408.

88 L. Xu, Y. Li, Q. Pan, D. Wang, S. Li, G. Wang, Y. Chen, P. Zhu and W. Qin, Dual-mode light-emitting lanthanide metal–organic frameworks with high water and thermal stability and their application in white LEDs, *ACS Appl. Mater. Interfaces*, 2020, **12**, 18934–18943.

89 B. Yan, Lanthanide-functionalized metal–organic framework hybrid systems to create multiple luminescent centers for chemical sensing, *Acc. Chem. Res.*, 2017, **50**, 2789–2798.

90 D. Yang, L. Lu, S. Feng and M. Zhu, First Ln-MOF as a trifunctional luminescent probe for the efficient sensing of aspartic acid, Fe³⁺ and DMSO, *Dalton Trans.*, 2020, **49**, 7514–7524.

91 J.-M. Li, R. Li and X. Li, Construction of metal–organic frameworks (MOFs) and highly luminescent Eu(III)-MOF for the detection of inorganic ions and antibiotics in aqueous medium, *CrystEngComm*, 2018, **20**, 4962–4972.

92 K. Ren, S.-H. Wu, X.-F. Guo and H. Wang, Lanthanide organic framework as a reversible luminescent sensor for sulfamethazine antibiotics, *Inorg. Chem.*, 2019, **58**, 4223–4229.

93 M.-L. Han, G.-X. Wen, W.-W. Dong, Z.-H. Zhou, Y.-P. Wu, J. Zhao, D.-S. Li, L.-F. Ma and X. Bu, A heterometallic sodium–europium-cluster-based metal–organic framework as a versatile and water-stable chemosensor for antibiotics and explosives, *J. Mater. Chem. C*, 2017, **5**, 8469–8474.

94 H.-W. Yang, P. Xu, B. Ding, Z.-Y. Liu, X.-J. Zhao and E.-C. Yang, A highly stable luminescent Eu-MOF exhibiting efficient response to nitrofuran antibiotics through the inner filter effect and photoinduced electron transfer, *Eur. J. Inorg. Chem.*, 2019, 5077–5084.

95 M.-Y. Jiang, L. Yu, Y.-C. Zhou, J. Jia, X.-J. Si, W.-W. Dong, Z.-F. Tian, J. Zhao and D.-S. Li, A novel d-f heterometallic Cdᴵᴵ-Euᴵᴵᴵ metal-organic framework as a sensitive luminescent sensor for the dual detection of ronidazole and 4-nitrophenol, *Z. Anorg. Allg. Chem.*, 2020, **646**, 268–274.

96 J.-M. Li, R. Huo, X. Li and H.-L. Sun, Lanthanide–organic frameworks constructed from 2,7-naphthalenedisulfonate

and 1*H*-imidazo[4,5-*f*,][1,10]-phenanthroline: Synthesis, structure, and luminescence with near-visible light excitation and magnetic properties, *Inorg. Chem.*, 2019, **58**, 9855–9865.

97 Q.-Q. Zhu, H. He, Y. Yan, J. Yuan, D.-Q. Lu, D.-Y. Zhang, F. Sun and G. Zhu, An exceptionally stable TbIII-based metal–organic framework for selectively and sensitively detecting antibiotics in aqueous solution, *Inorg. Chem.*, 2019, **58**, 7746–7753.

98 Z.-H. Zhou, W.-W. Dong, Y.-P. Wu, J. Zhao, D.-S. Li, T. Wu and X.-H. Bu, Ligand-controlled integration of Zn and Tb by photoactive terpyridyl-functionalized tricarboxylates as highly selective and sensitive sensors for nitrofurans, *Inorg. Chem.*, 2018, **57**, 3833–3839.

99 J. Zhang, L. Gao, Y. Wang, L. Zhai, X. Niu and T. Hu, A bifunctional 3D Tb-based metal–organic framework for sensing and removal of antibiotics in aqueous medium, *CrystEngComm*, 2019, **21**, 7286–7292.

100 F. Guo, C. Su, Y. Fan and W. Shi, An excellently stable TbIII–organic framework with outstanding stability as a rapid, reversible, and multi-responsive luminescent sensor in water, *Dalton Trans.*, 2019, **48**, 12910–12917.

101 J.-H. Wei, J.-W. Yi, M.-L. Han, B. Li, S. Liu, Y.-P. Wu, L.-F. Ma and D.-S. Li, A water-stable terbium(III)-organic framework as a chemosensor for inorganic ions, nitro-containing compounds and antibiotics in aqueous solutions, *Chem. – Asian J.*, 2019, **14**, 3694–3701.

102 H.-W. Yang, P. Xu, X.-G. Wang, X.-J. Zhao and E.-C. Yang, A highly stable (4,8)-connected Tb-MOF exhibiting efficiently luminescent sensing towards nitroimidazole antibiotics, *Z. Anorg. Allg. Chem.*, 2020, 23–29.

103 S. Wu, M. Zhu, Y. Zhang, M. Kosinova, V. P. Fedin and E. Gao, A water-stable lanthanide coordination polymer as multicenter platform for ratiometric luminescent sensing antibiotics, *Chem. – Eur. J.*, 2020, **26**, 3137–3144.

104 J. Song, X. Gao, Z.-N. Wang, C.-R. Li, Q. Xu, F.-Y. Bai, Z.-F. Shi and Y.-H. Xing, Multifunctional uranyl hybrid materials: Structural diversities as a function of pH, luminescence with potential nitrobenzene sensing, and photoelectric behavior as *p*-type semiconductors, *Inorg. Chem.*, 2015, **54**, 9046–9059.

105 L.-L. Liang, R.-L. Zhang and J.-S. Zhao, Counterion-controlled formation of layered honeycomb and polythreading uranyl networks and the highly sensitive and selective detection of Fe^{3+} in aqueous media, *Inorg. Chem.*, 2020, **59**, 7980–7990.

106 L. Wang, B. Tu, W. Xu, Y. Fu and Y. Zheng, Uranyl organic framework as a highly selective and sensitive turn-on and turn-off luminescent sensor for dual functional detection arginine and MnO_4^-, *Inorg. Chem.*, 2020, **59**, 5004–5017.

107 L. Wang, W. Xu, W.-Y. Li, M. Xie and Y.-Q. Zheng, A water-stable uranyl organic framework as a highly selective and sensitive bifunctional luminescent probe for Fe^{3+} and tetracycline hydrochloride, *Chem. – Asian J.*, 2019, **14**, 4246–4254.

108 H. He, F. Sun, T. Borjigin, N. Zhao and G. Zhu, Tunable colors and white-light emission based on a microporous luminescent Zn(II)-MOF, *Dalton Trans.*, 2014, **43**, 3716–3721.

109 R. Li, S. Li, J. Wang, J. Xu, C. Xu, J. Wang, C. Li and Z. Li, Facile generation of carbon quantum dots in MIL-53(Fe) particles as localized electron acceptors for enhancing their photocatalytic Cr(VI) reduction, *Inorg. Chem. Front.*, 2018, **5**, 3170–3177.

110 L. Liu, Z. Yao, Y. Ye, C. Liu, Q. Lin, S. Chen, S. Xiang and Z. Zhang, Enhancement of intrinsic proton conductivity and aniline sensitivity by introducing dye molecules into the MOF channel, *ACS Appl. Mater. Interfaces*, 2019, **11**, 16490–16495.

111 H. Pan, S. Wang, X. Dao and Y. Ni, Fluorescent Zn-PDC/Tb^{3+} coordination polymer nanostructure: A candidate for highly selective detections of cefixime antibiotic and acetone in aqueous system, *Inorg. Chem.*, 2018, **57**, 1417–1425.

112 Y. Yang, L. Zhao, M. Sun, P. Wei, G. Li and Y. Li, Highly sensitive luminescent detection toward polytypic antibiotics by a water-stable and white-light-emitting MOF-76 derivative, *Dyes Pigm.*, 2020, **180**, 108444.

113 Y.-Q. Zhang, X.-H. Wu, S. Mao, W.-Q. Tao and Z. Li, Highly luminescent sensing for nitrofurans and tetracyclines in water based on zeolitic imidazolate framework-8 incorporated with dyes, *Talanta*, 2019, **204**, 344–352.

114 K. Xing, R. Fan, X. Du, X. Zheng, X. Zhou, S. Gai, P. Wang and Y. Yang, Dye-insertion dynamic breathing MOF as dual-emission platform for antibiotics detection and logic molecular operation, *Sens. Actuators, B*, 2019, **288**, 307–315.

115 H.-R. Fu, L.-B. Yan, N.-T. Wu, L.-F. Ma and S.-Q. Zang, Dual-emission MOF ⊃ dye sensor for ratiometric fluorescence recognition of RDX and detection of a broad class of nitro-compounds, *J. Mater. Chem. A*, 2018, **6**, 9183–9191.

116 Y.-M. Ying, C.-L. Tao, M. Yu, Y. Xiong, C.-R. Guo, X.-G. Liu and Z. Zhao, *In situ* encapsulation of pyridine-substituted tetraphenylethene cations in metal–organic framework for the detection of antibiotics in aqueous medium, *J. Mater. Chem. C*, 2019, **7**, 8383–8388.

117 M. Yu, Y. Xie, X. Wang, Y. Li and G. Li, Highly water-stable dye@Ln-MOFs for sensitive and selective detection toward antibiotics in water, *ACS Appl. Mater. Interfaces*, 2019, **11**, 21201–21210.

118 K. Zhu, R. Fan, X. Zheng, P. Wang, W. Chen, T. Sun, S. Gai, X. Zhou and Y. Yang, Dual-emitting dye-CDs@MOFs for selective and sensitive identification of antibiotics and MnO_4^- in water, *J. Mater. Chem. C*, 2019, **7**, 15057–15065.

119 J. V. Alemán, A. V. Chadwick, J. He, M. Hess, K. Horie, R. G. Jones, P. Kratochvíl, I. Meisel, I. Mita, G. Moad, S. Penczek and R. F. T. Stepto, Definitions of terms relating to the structure and processing of sols, gels, networks, and inorganic-organic hybrid materials (IUPAC

Recommendations 2007), *Pure Appl. Chem.*, 2007, **79**, 1801–1829.

120 P. Sutar and T. K. Maji, Recent advances in coordination-driven polymeric gel materials: design and applications, *Dalton Trans.*, 2020, **49**, 7658–7672.

121 Z.-S. Qin, W.-W. Dong, J. Zhao, Y.-P. Wu, Z.-F. Tian, Q. Zhang and D.-S. Li, Metathesis in metal-organic gels (MOGs): A facile strategy to construct robust fluorescent Ln-MOG sensors for antibiotics and explosives, *Eur. J. Inorg. Chem.*, 2018, 186–193.

122 Z.-S. Qin, W.-W. Dong, J. Zhao, Y.-P. Wu, Q. Zhang and S. Li, A water-stable Tb(III)-based metal–organic gel (MOG) for detection of antibiotics and explosives, *Inorg. Chem. Front.*, 2018, **5**, 120–126.

123 X. Lian and B. Yan, Diagnosis of penicillin allergy: a MOFs-based composite hydrogel for detecting β-lactamase in serum, *Chem. Commun.*, 2019, **55**, 241–244.

124 F. Zhang, H. Yao, T. Chu, G. Zhang, Y. Wang and Y. Yang, A lanthanide MOF thin-film fixed with Co_3O_4 nano-anchors as a highly efficient luminescent sensor for nitrofuran antibiotics, *Chem. – Eur. J.*, 2017, **23**, 10293–10300.

125 Y. Gao, G. Yu, K. Liu and B. Wang, Luminescent mixed-crystal Ln-MOF thin film for the recognition and detection of pharmaceuticals, *Sens. Actuators, B*, 2018, **257**, 931–935.

126 C. Li, C. Zeng, Z. Chen, Y. Jiang, H. Yao, Y. Yang and W.-T. Wong, Luminescent lanthanide metal-organic framework test strip for immediate detection of tetracycline antibiotics in water, *J. Hazard. Mater.*, 2020, **384**, 121498.

127 F. Zhang, H. Yao, Y. Zhao, X. Li, G. Zhang and Y. Yang, Mixed matrix membranes incorporated with Ln-MOF for selective and sensitive detection of nitrofuran antibiotics based on inner filter effect, *Talanta*, 2017, **174**, 660–666.

128 C. Li, F. Zhang, X. Li, G. Zhang and Y. Yang, A luminescent Ln-MOF thin film for highly selective detection of nitroimidazoles in aqueous solutions based on inner filter effect, *J. Lumin.*, 2019, **205**, 23–29.

129 F. Zhang, J. Ma, S. Huang and Y. Li, A mechanical stability enhanced luminescence lanthanide MOF test strip encapsulated with polymer net for detecting picric acid and macrodantin, *Spectrochim. Acta, Part A*, 2020, **228**, 117816.